

Paleoglaciology of the central East Antarctic Ice Sheet is revealed by blue-ice sediment

We present ~100 cosmogenic ages for a blue-ice moraine at Mt. Achnar, central Transantarctic Mountains.

The Law Glacier surface experienced relatively minor fluctuations in surface elevation throughout MIS 6 and 5, and likely previous.

A lateral moraine indicates the Law Glacier surface was higher at $\sim 9.2 \pm 0.5$ ka.

Blue-ice sediments are an underutilized and dateable paleoglaciologic and paleoclimate archive

1 Paleoglaciology of the central East Antarctic Ice Sheet as revealed by
2 blue-ice sediment

3
4 **Kaplan, M.R.^{1*}, Licht, K.J.², Lamp, J.L.¹, Winckler, G.^{1,3}, Schaefer, J.M.^{1,3}, Graly, J.A.⁴,
5 Kassab C.M.², Schwartz, R.¹**

6 ¹*Geochemistry, Lamont-Doherty Earth Observatory, Palisades, New York 10964, USA*

7 ²*Department of Earth Sciences, IUPUI, Indianapolis, Indiana 46202, USA*

8 ³*Department of Earth and Environmental Sciences, Columbia University, New York, New York
9 10027, USA*

10 ⁴*Department of Geography and Environmental Science, Northumbria University, Newcastle-
11 Upon-Tyne, NE1 8ST, UK*

12
13 *E-mail: mkaplan@ldeo.columbia.edu

14
15 *Corresponding author: mkaplan@ldeo.columbia.edu

16
17 **Keywords:** cosmogenic dating; Law Glacier; Holocene; Antarctica; paleoclimate, Pleistocene;
18 deglaciation

19
20 **Abstract**

21 We present ~100 cosmogenic surface exposure ages, including 75 new analyses, for a blue-ice
22 moraine complex at Mt. Achnernar, head of Law Glacier, in the central Transantarctic Mountains.
23 The ¹⁰Be-³He-²⁶Al ages along with previously-published boron concentrations chronicle past
24 behavior of the East Antarctic Ice Sheet (EAIS) along the edge of the polar plateau since the
25 sediments started to accumulate, around 0.5-1 Ma. Sediments analyzed for ¹⁰Be from the Law
26 Glacier surface record <100 years of exposure, indicating they likely have negligible inheritance
27 when first exposed. The Law Glacier surface experienced relatively minor fluctuations in surface
28 elevation throughout MIS 6 and 5, and likely during prior periods, as geomorphic features are
29 intact and exposure ages are coherent on the moraine, ranging from ~210 to ~86 ka; respective
30 means for MIS 5 sediments in two different areas are 106±9.1 ka [n=4 ages] and 106±5.1 ka [n=6].
31 Although we infer the Law Glacier has been relatively close to its current configuration generally
32 since 0.5-1 Ma, disturbances to Achnernar blue-ice moraine architecture seem apparent at times
33 especially prior to the last two glacial cycles. The largest observed disturbance occurred when the
34 nearby Lewis Cliffs Ice Tongue expanded either near, or much earlier than, 500-400 ka. A
35 minimum ice thickness increase of 30 m is associated with the ~20 ka blue-ice ridges, and a lateral
36 moraine indicates the Law Glacier surface was ~40-50 m higher at ~9.2±0.5 ka. Our findings
37 support that lateral accretion over time formed the Mt. Achnernar blue-ice moraine sequence, and
38 by implication, other analogue Antarctic deposits. We interpret blue-ice moraines as representing,
39 at times, relatively constant outlet glacier conditions and concur with prior studies that they reflect
40 near-equilibrium forms. Blue-ice sediments are an underutilized and dateable paleoglaciologic and
41 paleoclimate archive in Antarctica, including for former ice surface dynamics and possibly as a
42 repository of old ice during periods such as MIS 5 and prior.

43

44 **1. Introduction**

45 In paleoglaciology, former ice surfaces and their dynamics can be difficult to reconstruct
46 as evidence is not typically left behind. This is especially true for past ice sheet interiors, including
47 for those that still exist in Antarctica. In particular, observations of former ice sheet surfaces are
48 not common prior to the last local glacial maximum (LGM), including in Antarctica. Blue ice
49 ablation zones and their moraines are common throughout the Antarctic continental interior, and
50 provide a unique means to reconstruct the surfaces of former ice sheets, including prior to the LGM
51 (Bintanja, 1999). The primary reason is that their sediment accumulations overlie ice that is
52 adjacent to and linked into active glacier flow (Whillans and Cassidy, 1983; Cassidy et al., 1992;
53 Bintanja, 1999; Sinisalo and Moore, 2010).

54 Reconstructing past ice surface elevations is important for multiple reasons. First, we can
55 use such evidence to document the relative stability or instability of the interior of the EAIS and
56 other sectors of Antarctica, including during past warm periods. Second, blue-ice sediment and ice
57 arrive from below the surface (Whillans and Cassidy, 1983; Chinn, 1991, 1994; Cassidy et al.,
58 1992; Corti et al. 2008; Sinisalo and Moore, 2010; Palmer et al., 2012). Hence, their study
59 improves understanding of subglacial, englacial, and supraglacial processes, as well as underlying
60 geology that cannot be observed (Fogwill et al., 2012; Palmer et al., 2012; Ackert et al., 2013;
61 Campbell et al., 2013; Hein et al., 2016; Westoby et al., 2016; Winter et al., 2016; Bader et al.,
62 2017; Graly et al., 2018a,b, 2020;). Third, observations of past surfaces and outlet glacier behavior
63 provide test beds for model experiments (Pattyn, 2010; Whitehouse et al., 2012; Golledge et al.,
64 2013; DeConto and Pollard, 2016), including the sensitivity of different sectors of Antarctica to
65 past warm periods. Last, age information on past surfaces may reveal sites where old ice is
66 preserved (Higgins et al., 2015).

67 Detailed study of blue-ice sediments is required to understand better these features as
68 important paleoglaciologic and paleoclimate archives. Blue-ice areas typically occur under
69 compressive glaciological regimes where rates of sublimation and wind scouring exceed
70 accumulation. Studies in West Antarctica show that blue-ice regions offer a dateable archive of
71 former ice sheet behavior over the million year timescale (Fogwill et al., 2012; Hein et al., 2016;
72 Woodward et al. 2022). In the Transantarctic Mountains (TAM) blue-ice areas also provide
73 repositories of old ice (e.g., Higgins et al., 2015), because compressive stresses related to flow
74 around the Transantarctic Mountains and sublimation rates bring subglacial and englacial ice
75 towards the surface from lower, older sections of the ice sheets (Whillans and Cassidy, 1983; Corti
76 et al., 2008).

77 Here, we provide ^{10}Be - ^3He - ^{26}Al cosmogenic surface exposure ages near Mt. Achnernar in
78 the central TAM and synthesize all chronologic data with prior efforts in the area (Figs, 1, 2). We
79 use the findings to answer questions concerning the timing, amount, and stability of former ice
80 surface changes at the head of the Law Glacier (Fig. 1) at the edge of the polar plateau, where ice
81 converges into the central TAM. Model output shows that this sector of the EAIS may be relatively
82 insensitive to past climate changes including warm periods (e.g., DeConto and Pollard, 2016). The
83 data allow us to evaluate whether such simulations are consistent with observations, specifically
84 those documenting the magnitude of changes if the central EAIS has been relatively stable.

85

86 **2. Background**

87 *2.1. Mt. Achnernar setting*

88 The Mt. Achnernar blue-ice moraine complex begins approximately 20 km downstream of
89 the EAIS plateau. The blue-ice area exists at the head of Law Glacier, which is between the Queen

90 Alexandra and Queen Elizabeth Ranges. Topographic steering into a lee-side embayment (Fig. 1)
91 downstream of Mt. Achnar (2691 m) traps upward flowing ice in a blue-ice area, which
92 subsequently sublimates. Near the active Law Glacier ice/moraine edge (Fig. 3) subsurface-
93 derived debris bands are emerging parallel/subparallel to the margin, and document how en- and
94 subglacial sediment is added to the moraine (Kassab et al., 2019).

95 The Achnar blue-ice moraine is $\sim 100 \text{ km}^2$ and extends $>5 \text{ km}$ from the active Law
96 Glacier towards the Lewis Cliffs Ice Tongue and other unnamed glaciers that flow more or less
97 northward in the opposite direction (Fig. 1). Located around an elevation of 1700-1900 m, the
98 majority of the moraine complex is dominated by a series of 1-12 m high ridges and troughs that
99 run subparallel to the main flow direction of Law Glacier (Bader et al., 2017). Ridge orientation
100 commonly mimics the shape of the active main trunk of Law Glacier (Fig. 1). Some ridges exhibit
101 laterally continuous visible bands and till of sandstone, dolerite, or mixed lithologies that impart a
102 generally consistent color (Fig. 4), which often provides a strategy for sampling. On sunny or
103 relatively warm days with air temperatures still below freezing, we observed surface melting
104 associated with dark-colored debris, especially near the boundary between the moraine and the
105 clean ice of Law Glacier. Although seemingly minor in terms of quantity, we assume such melting
106 may have important geomorphological effects (Graly et al., 2018b) (Fig. 3).

107

108 *2.1.1. Prior studies at Mt. Achnar*

109 Early studies of the Mt. Achnar area, including the Lewis Cliffs Ice Tongue and Walcott
110 N  v  , were conducted due to the site's usefulness for meteorite collection (e.g., Faure et al. 1992;
111 Cassidy et al., 1992; Hagen, 1995). Scarrow et al. (2014) studied soil chronosequences and patterns
112 of moraine development in this arid setting and inferred that through time material is added so as

113 to thicken progressively the soil from its base, which was documented in later as studies as well
114 (Bader et al., 2017; Graly et al., 2018b). Near the Lewis Cliffs Ice Tongue, Sun et al. (2015)
115 focused on the geochemistry of salts emerging from subglacial water, and argued for a sustained
116 cold polar environment for millions of years.

117 Bader et al. (2017) presented geomorphic, sedimentologic, and till composition and
118 provenance findings including pebble lithology and detrital zircon geochronology, for the Mt.
119 Achernar moraine complex. They defined 5 zones of the moraine sequence – which we follow in
120 this study – based on color bands and distinct differences in geomorphology; Bader et al (2017)
121 also found the zones coincided with the relative weathering of sediments and their provenance
122 characteristics. Briefly, Zone 1 tends to be hummocky with pronounced pond-like depressions
123 separated by ridges (Fig. 3). The ridges and depressions exhibit in places a weak alignment that is
124 oriented more or less at an oblique angle to the ice margin (Figs. 1D, 3). Sediments are grey or
125 dark grey. Zone 2 is distinguished by relatively low relief with small ridges far apart (Fig. 4). Zones
126 3 & 4 contain well-defined continuous parallel/sub-parallel ridges and troughs (Fig. 4). Zone 4
127 contains sediments that are pale yellow or light-yellowish brown characteristic of weathering of
128 sandstones, or red varnish that is associated with weathering of the Ferrar Dolerite (Mercer, 1968).
129 Zone 5 sediment exhibits extensive red varnish and consists of parallel/sub-parallel ridges sourced
130 in part from an unnamed northward flowing glacier. In Zone 5, two reported ^3He exposure ages
131 are recalculated from Kaplan et al. (2017), and the boron data are from Graly et al. (2018a).

132 In the downglacier (northeast) part of the area studied, referred to as the tail, a prominent
133 moraine ridge exhibits characteristics similar to Zone 1 (Bader et al., 2017) (Figs. 2, 5, 6). Past the
134 moraine ridge (i.e., farther from Law Glacier) exists a snow-covered gap (<20 m wide) and then
135 topographic moraine ridges/troughs. In places, the ridges exhibit a change in orientation so that

136 they are oblique to the innermost moraine ridge (Figs. 1D, 2). On the other side of the snow-
137 covered gap, sediments are pale yellow or light yellowish brown or dark red (Ferrar Dolerite)
138 similar to in Zone 4 along the main transect; hence, just based on moraine description we conclude
139 the gap represents a significant temporal discontinuity (Bader et al., 2017; Graly et al., 2018a).

140 Bader et al. (2017) also described facets and striations on up to 30% of the cobble clasts
141 indicating an active subglacial origin, and concluded that blue-ice sediments contain a valuable
142 record of underlying unexposed bedrock geology that cannot be directly observed. Given there is
143 no exposed bedrock upstream of Mt. Achernar, the moraine sediment is subglacially or englacially
144 derived with mostly local but also some non-local components (Bader et al., 2017), except for
145 meteorites (Cassidy et al, 1992). Over the time interval represented by the moraine complex, Bader
146 et al. (2017) inferred former ice surface changes of <40 m and relatively stable past ice sheet
147 configurations, in part based on the geomorphology and compositional and provenance studies of
148 glacial till and pebbles.

149 The first direct chronologies for the Mt. Achernar moraine (Hagen, 1995; Kaplan et al.,
150 2017) established that the site contains sediments exposed at the surface since before the global
151 LGM, during Marine Isotope Stage 2 (MIS 2). Bader et al. (2017) and Kaplan et al (2017) inferred
152 the East Antarctic polar plateau has been relatively stable for at least 200 kyr. Graly et al. (2018a)
153 analyzed salt concentrations and speciation in the top horizons of Mt. Achernar sediments. They
154 found the concentration of boron-containing salts are highly correlated to exposure ages of nearby
155 boulders from the same moraine ($R^2 >0.99$) and inferred that low vapor pressure at cold
156 temperatures and extreme aridity limit mobility of such salt species within the soil column, and
157 major melt could not have occurred during the time the moraine existed. By calibrating boron
158 concentrations in till soils to the first set of cosmogenic nuclide ages available from nearby

159 boulders, Graly et al. (2018a) documented that boron concentration provides a sediment exposure
160 age, which is used in this study.

161 Most recent studies at Mt. Achnar provided insights into regional subglacial and englacial
162 processes, and general blue-ice moraine sediment formation and soil chemistry. Kassab et al.
163 (2020) integrated ground-penetrating radar (GPR, 100 and 25 MHz) data with GPS measured ice
164 velocity and published surface exposure ages (Kaplan et al, 2017; Graly et al., 2018a). GPR
165 transects (100 and 25 MHz) both perpendicular and parallel to moraine ridges revealed alternating
166 relatively clean ice and horizons where englacial debris bands dip steeply towards the surface.
167 Kassab et al. (2020) suggested sediment generally moves upward associated with debris bands
168 (and along shear planes?), but in certain locations there are more complicated subsurface
169 structures. Kassab et al. (2020) also documented that the entire moraine is underlain by >150 m
170 glacier ice, with varying amounts of debris in places including in the englacial bands. Along with
171 Graly et al. (2018b), they estimated a maximum elapsed time of ~100-250 kyr from subglacial
172 entrainment to transport and debris reaching the surface. Kassab et al. (2020) proposed a model to
173 explain the formation of blue-ice moraine sequences whereby debris accretes laterally to form new
174 moraine. They also inferred englacial sediments may continue to accumulate at the base of the
175 already-existing moraine, agreeing with the earlier study of Scarrow et al. (2014). Using oxygen
176 isotopes, including those from a shallow core, Graly et al. (2018b) documented that glacier ice
177 flowing upward into the Achnar moraine system was sourced from the EAIS plateau (Fig. 1),
178 and inferred ice and sediment entrainment in an open system under warm-based basal conditions.
179 Graly et al. (2018b) estimated a minimum age of MIS 6 for the ice underlying and feeding the
180 Achnar blue-ice moraine, and that ice within the current Law Glacier was slightly younger and
181 originated during MIS 5. Last, prior papers argued that the lateral continuity of the ridges and

182 troughs, specifically those with distinct lithologies (Figs. 2, 4), exposure age progression, and
183 general geochemistry and till provenance signify relative stability of the moraine surface (e.g.,
184 Bader et al., 2017; Kaplan et al., 2017; Graly et al., 2018a,b, 2020).

185

186 **3. Methods**

187 We conducted field work at Mt. Achernar during the 2011 and 2015/16 austral summers,
188 either from a nearby base camp ~6 to 20 km from the moraine sampling sites, or by several 1-day
189 trips by helicopter from the larger CTAM (central TAM) camp. Samples for cosmogenic exposure
190 analyses were collected in three parts of the moraine complex: 1) near and along the main part of
191 the moraine sequence. A main transect, as indicated by the dashed-white line in Figure 2, is where
192 the majority of samples were collected, and was largely the focus of earlier studies by our group;
193 2) in the downglacier (southwest) part of the study area, in an area informally referred to as the tail
194 (Figs. 2, 5); 3) along a lateral moraine that runs along the headwall of Mt. Achernar (Figs. 4, 6).

195 We collected quartz-bearing sandstones and pyroxene-bearing dolerites for ^{10}Be - ^{26}Al and
196 ^3He , respectively. We sampled mainly boulders (> 25 cm high), but also cobbles as noted in the
197 figures and tables. We preferentially selected boulders away from depressions (e.g., polygon
198 boundaries) in areas where periglacial processes were apparent. Samples were taken from the
199 upper 1-3 cm of the boulder, in the most stable-looking, horizontal/flat portion (and if possible as
200 close to the center as possible) of the top surface. Samples were collected with hammer and chisel.
201 A compass and clinometer were used to measure the azimuthal elevations of the surrounding
202 landscape to account for shielding, although it was negligible in almost all cases except for the
203 four lateral moraine samples (~1-1.5% difference in exposure age).

204 We used a handheld GPS (WGS 84) for all sample latitudes and longitudes. For sample
205 elevations, we used a Trimble GPS system (EGM96), except for 9 sandstones (^{10}Be - ^{26}Al) and 4
206 dolerites (^3He) as noted in Table 1. Differential processing used continuous data from a permanent
207 base station set up on a bedrock surface that was 8 km (tail) to 20 km (lateral moraine on Fig. 2)
208 away. For latitude and longitude, we checked all handheld GPS measurements against post-
209 processed differential-based analyses where available, and as expected they are indistinguishable
210 at the scale of all the figures. For elevation, we assume uncertainties are <1 m if differentially
211 based. Comparison of handheld GPS data with differential-based elevations for 104 sites, in which
212 both are available, yields an average offset of $+9.1\pm 4.1$ m, excluding one sample that was +47.8
213 m higher. Except for two samples, the handheld GPS always gave higher elevations. Four samples
214 on one particular moraine ridge were only measured with a handheld GPS, and as noted below in
215 the Results their recorded elevations may be ~10 m too high relative to EGM96 orthometric
216 heights; if correct, this would cause these 4 exposure ages to be <1% too low.

217 Processing for ^{10}Be preparation and analyses followed standard procedures at the Lamont
218 Cosmogenic Nuclide Laboratory (Schaefer et al., 2009; Kaplan et al. 2017). A custom-made ^9Be
219 carrier allows measurement of samples with extremely low concentrations, 1000-2000 ^{10}Be
220 atoms/g (Table 1). Almost all samples were measured at the Center for Accelerator Mass
221 Spectrometry at Lawrence Livermore National Lab, except for nine samples associated with blank
222 BLK2017May10 (Table 1), which were analyzed at PRIME Lab. All ^{26}Al analyses in this
223 manuscript are from Kaplan et al. (2017), although they were recalculated with up-to-date
224 systematics.

225 All reported exposure ages were calculated using Version 3 of the online cosmogenic
226 exposure age calculator hosted by the University of Washington (<https://hess.ess.washington.edu>)

227 (Balco et al., 2008), including ages updated from Kaplan et al. (2017) and Hagen (1995). ^{10}Be and
228 ^{26}Al ages are presented based on the production rate calibration dataset from Kaplan et al. (2011)
229 for $\sim 50^\circ\text{S}$ in southern South America, which is the closest geographically to Antarctica. This rate
230 is statistically indistinguishable from the other middle latitude Southern Hemisphere ^{10}Be
231 production rate calibration, derived in the Southern Alps of New Zealand at $\sim 43^\circ\text{S}$ (Putnam et al.,
232 2010). We present results using three latitude and elevation-dependent production rate scaling
233 methods (St, Lm, LSDn) (Table 3), although for the sake of discussion we show and discuss the
234 time dependent version of Lal (1991)/Stone (2000) (Lm) except where noted.

235 A recent study by Balter et al. (2020) presented evidence that (at least) at high elevation
236 Antarctic sites and for samples exposed continuously for $>10^6$ years, the production rate calibration
237 dataset of Borchers et al. (2016) and the LSDn scaling method (Lifton et al., 2014) are perhaps
238 most appropriate for calculating exposure ages. In the Discussion, we also provide ages derived
239 with the rate in Borchers et al. (2016) and LSDn scaling where it may slightly affect our inferences,
240 specifically for the oldest exposure ages. Although we present and discuss ages using the Lm (Lal,
241 1991; Stone, 2000), Table 2 shows differences if LSDn (Lifton et al., 2014) is used instead. For
242 almost all cosmogenic ages, LSDn scaling affords $\sim 10\%$ younger ages than Lm, except for samples
243 exposed for ~ 1000 - 2000 years (13 - 14% younger) and for the last 100 years (0 to 5% older). If the
244 ^{10}Be production rate dataset in Borchers et al (2016) is used instead of the middle latitude Southern
245 Hemisphere dataset (Kaplan et al. 2011; *cf.*, Putnam et al., 2010), the exposure ages become 5%
246 and 2% lower using the Lm and LSDn scaling methods respectively.

247 Processing of pyroxene separates and ^3He analyses followed standard procedures at the
248 Lamont Cosmogenic Nuclide Laboratory (Bromley et al., 2014; Eaves et al., 2015, 2016; Kaplan
249 et al. 2017). Abundance and isotopic analyses are performed with a MAP215-50 noble gas mass

250 spectrometer. Analyses are against either a known volume of a Yellowstone helium standard
251 (MM), or air, as noted in Table 2. As in the case of ^{10}Be and ^{26}Al , we used Version 3 of the online
252 calculator at <https://hess.ess.washington.edu> (Balco et al., 2008) to calculate new, and recalculate
253 previously published (e.g., Kaplan et al., 2017), ^3He exposure ages. Analogous to ^{10}Be and ^{26}Al ,
254 we present results from three scaling methods (Table 3), although we show and discuss ages
255 derived with L_m , the time-dependent version of Lal (1991)/Stone (2000), except where noted.
256 Eaves et al. (2015) examined the cosmogenic $^3\text{He}_{\text{px}}$ production rate in the south-west Pacific (39°S)
257 and found it indistinguishable from the default production rate calibration dataset of Borchers et
258 al. (2016).

259 ^3He concentrations and resulting exposure ages presented here are not corrected for
260 noncosmogenic (nucleogenic and inherited mantle-derived) ^3He in the samples. Unlike in Kaplan
261 et al. (2017), we do not report ^3He ages with and without subtracting an inferred inherited or
262 nucleogenic fraction. Kaplan et al. (2017) and Balco (2020) suggested noncosmogenic
263 concentrations roughly in the mid- 10^6 atoms/g range consistent with prior estimates (e.g., Ackert,
264 2000). As most of the ^3He exposure ages presented here contain 10^7 - 10^8 atoms/g (i.e., >10 ka,
265 Tables 2 and 4), the effect is not significant in terms of our findings and conclusions. A future
266 manuscript will discuss such ^3He corrections at Mt. Achnar.

267 All cosmogenic nuclide exposure ages reported in Tables 3 and 4 assume no erosion. As
268 Antarctica has some of the lowest erosion rates on Earth (Schäfer et al., 1999), for most samples
269 we assume erosion is insignificant. In fact, some of the boulders are still striated (e.g., <10 ka).
270 Nonetheless, we point out that if we assume an erosion rate of ~ 10 cm Ma^{-1} , the ~ 500 ka ages
271 (oldest) increase by $\sim 5\%$. Also, we do not correct for snow cover on the boulders. We point out
272 that by definition blue-ice areas contain generally little or no snow (Bintanja, 1999). Although

273 some snow may accumulate in small depressions, we avoided sampling in such spots. Hagen
274 (1995) noted that their one prominent young exposure age outlier of ~15 ka could be explained by
275 the fact it was collected from a depression with snow (Fig. 2), as mentioned in Kaplan et al. (2017).

276

277 **4. Results**

278 For the ease of presentation, below we describe results separately for three parts of the Mt.
279 Achernar area: the main moraine sequence, the tail area, and the lateral moraine along the headwall
280 of Mt. Achernar (labeled on Fig. 2). In addition, we refer to Zones 1 to 5, as first described in
281 Bader et al. (2017) and elaborated on in Kassab et al. (2020) and reviewed above in Section 2.2.
282 Furthermore, Graly et al. (2018a) sampled several moraines for boron concentrations (Fig. 1c) that
283 were not dated in this study with ^{10}Be - ^3He - ^{26}Al . The calibrated boron approach thus adds to the
284 exposure chronology of the entire moraine system (Fig. 7), and ages are mentioned here in Results
285 where pertinent.

286

287 *4.1. Main part of moraine sequence (Figs. 2-4, 6-7)*

288 Most measured samples come from boulders (and 3 cobbles) located close to a transect that
289 was the focus of prior studies, shown by the white-dashed line in Figure 2. In Zone 1, we analyzed
290 three samples associated with active, relatively clean Law Glacier ice, near the contact with the
291 moraine (Fig. 3). A boulder yields a ^{10}Be exposure age of 79 ± 5 yrs, and two cobble-sized samples
292 52 ± 4 and 76 ± 8 yrs; thus samples near the Law margin record <100 years of apparent exposure.
293 Two nearby samples around the ice/moraine contact but on the moraine have ^{10}Be ages ~600-1000
294 years (MAR-15-110, -111); these results are consistent with two ^{10}Be ages just to the east (Fig.
295 2B; MAR-15-139, -142h), near a small embayment in the moraine, which give essentially identical

296 ages, ~800-700 years for apparent exposure. Inward, along Zone 1 sediment (Figs. 3,7), exposure
297 ages steadily increase to around 10 ka. Three dolerites yield apparent ^3He ages of ~7 ka and ~14
298 ka (MAR-11-01,-02, -112c), the first two of which were previously published. As Kaplan et al.
299 (2017) noted, these three apparent exposure ages may record primarily non-cosmogenic ^3He
300 concentrations, with some cosmogenic component given their presence in Zone 1. Given the large
301 uncertainty for MAR-15-61 (>20%), its age of 2.8 ± 0.7 ka is not used (Table 1).

302 In Zone 2, exposure ages remain around 14-10 ka, with one discordant ^{26}Al age slightly
303 older. In Zone 3, ages increase to ~55 ka (Figs. 4,7). This includes four coherent ages dating to
304 19.3 ± 0.8 (excluding one outlier of ~5.9 ka), and a cluster between ~55 and 35 ka (excluding one
305 outlier of ~14.3 ka). We note at least six ridges remain undated in Zone 3.

306 In Zone 4, we sampled ~5-6 ridges. Exposure ages begin around 100 ka and steadily
307 increase (Figs. 2,7). Four coherent ages date to 106 ± 5.1 ka; in addition, two younger ages on
308 different samples are 57.8 ± 3.0 and 39.9 ± 1.7 ka, respectively, with the lowest age on a cobble-size
309 rock. Slightly farther away from the Law Glacier to the southeast, two ages are 135.2 ± 2.2 and
310 120.0 ± 2.5 and one nearby younger age is 86.1 ± 1.3 . A cluster of ages ranges from ~213 to 177 ka,
311 along with one younger age of 73.7 ± 4.3 ka. The oldest ^{10}Be - ^{26}Al ages towards the back of Zone 4
312 are ~530-450 ka. The oldest ^3He age is ~380 ka. One cobble-size sample near the ~500 ka boulder
313 dates to ~370 ka. The boron analyses are consistent with ~500 kyr, or possibly 500-400 kyr, of
314 exposure (Fig. 7; Graly et al., 2018a). Close to the Lewis Cliffs Ice Tongue, exposure ages reverse
315 and become younger. Exposure ages reported in Hagen (1995) are consistent with the new data
316 (Fig. 2). We note that sample elevations for MAR-15-123 to 126 were measured only with a
317 handheld GPS, which tended to be ~10 to 9 m higher than differential-based elevations; if the
318 elevations are too high by ~10 m, the resulting exposure age would be typically $\leq 1\%$ too low,

319 which is within age uncertainties. In summary, we obtained a large number of ages around 210-
320 177 ka and 135-86 ka.

321 In Zone 5, which is farthest from the Law Glacier (Fig. 1C), two ^3He ages are 109 ± 3 ka
322 (MAR-11-48) and 316 ± 7 ka (MAR-11-52). The ~ 109 ka boulder is closer to the boundary of
323 sediments associated with the Lewis Cliffs Ice tongue (Fig. 2A), it is greyer in color and located
324 near material with less varnish, and it appears to be surrounded by depressions on the order of a
325 few meters that we assume are caused by periglacial processes. In contrast, the ~ 316 ka sample is
326 farther into Zone 5 (Fig. 2A) and surrounded by sediments with extensive red varnish. Closer to
327 the unnamed glacier, slightly farther south, Graly et al. (2018a) obtained boron exposure ages of
328 ~ 1 Ma and ~ 680 ka.

329 For the entire exposure age distribution in the main sampling area, an exponential relation
330 can describe the increase in ^{10}Be - ^3He - ^{26}Al -Boron ages with distance from relatively clean Law
331 Glacier ice (Fig. 7), with an $R^2 > 0.7$. For surface sediments exposed < 50 kyr, or up to ~ 2200 - 2000
332 m from Law ice, a linear relation also can be used to represent exposure age versus distance, with
333 an R^2 of ~ 0.8 (^{10}Be) or ~ 0.6 (^3He). That is, a break in slope, or a notable change in the samples'
334 exposure age versus their distance from Law Glacier occurs around 50 ka or at least prior to the
335 last glacial cycle.

336

337 *4.2. Tail area (Fig. 5)*

338 In the downglacier sector of Mt. Achernar, we analyzed samples from recently emerged
339 debris along the edge of the Law Glacier, from the prominent grey-colored, unoxidized moraine
340 positioned east of the ice-contact area, and also from the light-yellowish brown and red till located
341 on the other side (east) of the prominent snow gap (Figs. 2, 5, 6). Closest to relatively clean Law

342 ice is the youngest exposure age (320 years). A short distance away (~10 m) from Law Glacier
343 and slightly higher (about +4 m), ages increase to ~2700-1100 yrs, similar to those observed in the
344 main area (Figs. 2, 3). The prominent right lateral ice-cored moraine of gray till is continuous for
345 several kilometers and eventually dissipates downstream. On this moraine, we obtained a relatively
346 wide age distribution from ~1 ka to 18 ka. A boulder and cobble (MAR-15-132, -133) provided
347 ages of ~740 years and ~1.7 ka, respectively. Close to these two ages of <2 ka, and still on the grey
348 unoxidized moraine, is a boulder age of 15.1 ± 0.2 ka, and at the end of the tail is another boulder
349 age of 17.8 ± 0.3 ka. The two boulder ages ~15-18 ka are located in the last ~1,200 m before the
350 tail dissipates, and they do not appear to have a relation with distance from the Law ice edge; the
351 ~15.1 ka boulder is located slightly closer to the Law margin compared with the 1.7 ka sample.

352 East of the grey moraine by ~50 m, samples were collected from the light-yellowish brown
353 and red oxidized till. Here moraine ridges are oblique to the gray moraine and six ^{10}Be - ^3He dates
354 offer a coherent age cluster of 103.1 ± 8.9 ka, or 105.9 ± 5.1 ka excluding an age of 85.8 ± 1.7 ka, and
355 an obvious outlier of ~18.6 ka (Fig. 5). A second set of three ^3He ages slightly farther to the
356 southeast (MAR-11-41 to 43) date to 160-110 ka. There is a difference of about 60-80 kyr – close
357 to a full glacial cycle – between the light-yellowish brown/red oxidized and the unoxidized
358 moraine areas. The unoxidized and oxidized sediments are at similar elevations, with the latter (i.e.,
359 lateral moraine) being slightly higher by ~5-10 m. The light-yellowish brown and red oxidized
360 sector is about the same elevation as the modern ice surface, ~1750-1740 m (Fig. 5).

361

362 *4.3 Lateral moraine along headwall of Mt. Achnar.*

363 Four cobble-sized samples were ^{10}Be dated along a lateral moraine that runs along the west-
364 side headwall that bounds the Achnar moraine complex (Figs. 2,3). The ages form a relatively

365 coherent distribution with a mean age of 9.2 ± 0.5 ka. The moraine is approximately 40-50 m above
366 the current clean ice margin (Fig. 6D-F), and is oriented more or less in the direction of flow into
367 the lee side embayment and towards the Mt. Achnar moraine (Kassab et al., 2020), and oblique
368 to the flow of the trunk of Law Glacier (Fig. 1). The moraine slopes about 20m/km southeastward
369 towards the middle of the moraine complex and appears to end in inner Zone 4, just past the 100
370 ka ridges of the main area. There is a trimline that is higher than the lateral moraine, by <20m and
371 <10m close to Law Glacier and adjacent to inner Zone 4, respectively. This trimline remains
372 undated and is discussed further in Section 5.3.

373

374 *4.4 Boulders vs cobbles*

375 We sampled cobble-sized sediments to compare their exposure ages with those of boulders.
376 By the ice/moraine contact, one boulder and two cobbles have similar apparent exposure ages
377 (~80-50 yrs). In the back of Zone 4, one cobble-size sample (MAR-15-113c) was obtained near
378 the ~500 ka boulder and is notably younger (370 ± 7 ka). For comparison, the nearby boron
379 concentration is consistent with 500-400 kyr of exposure (Fig. 7; Graly et al., 2018a). In the tail
380 area, the cobble-sized sample (MAR-15-88) has a ^{10}Be result (~1.1 ka) consistent with other nearby
381 boulders and cobbles; in addition, it is slightly farther (~10-20 m) away from the sample exposed
382 for less time, ~320 yrs, and present clean ice edge (Figs. 5, 6).

383

384 *4.5 ^{26}Al and ^{10}Be comparison*

385 Kaplan et al. (2017) reported ten $^{26}\text{Al}/^{10}\text{Be}$ pairs, with one sample (MAR-11-14) measured
386 twice (Tables 2, 4) as well as 6 pairs previously from Hagen (1995). In general, the fifteen samples
387 do not contain substantial evidence for complex histories of burial and re-exposure (Fig. 8). Three

388 samples (~20%) plot just below the constant exposure line at 1σ (but not at 2σ). Taken at face
389 value, these three samples may contain evidence of some burial history. In more detail: 1) MAR-
390 11-33 gives a ^{10}Be age of 36.4 ± 0.5 ka, which is also one the younger ages of the distribution in
391 this part of the moraine (excluding an obvious outlier of ~12.9 ka), perhaps related to its relatively
392 short burial history; 2) The oldest sample measured, MAR-11-14, has discordant ^{10}Be - ^{26}Al ages
393 (529 ± 7 , 439 ± 10 , a result reproduced in the duplicate sample (532 ± 7 , 455 ± 11 ka). Two possible
394 analyses of MAR-11-14 (Fig. 8) include the following. (i) The sample plots along a line of
395 continuous exposure but with erosion causing concentrations close to saturation. Sandstones
396 exposed for 10^5 years may start to disintegrate, a finding noted in earlier studies (e.g., Denton et
397 al., 1993). (ii) Alternatively, MAR-11-14 also may exhibit some history of burial, or both erosion
398 and burial have produced the sample concentrations. The oldest sample in Hagen (1995) may also
399 have a similar history as MAR-11-14, with either some erosion or burial perhaps causing slightly
400 discordant ages (at 1σ , but not 2σ).

401

402 **5. Discussion**

403 *5.1 Chronology*

404 The Mt. Achnar area preserves one of the best-dated and coherent blue-ice moraine
405 sequences in East Antarctica. Statistically significant relations between distance and ^{10}Be - ^{26}Al -
406 ^3He -Boron exposure ages (Fig. 7) document a net increase in exposed time from the Law Glacier
407 margin. An exponential increase in exposure age versus distance from Law Glacier, especially >50
408 ka (Fig. 7A), implies shorter spacing between the older ridges (Kassab et al., 2020), or an amount
409 of original moraine morphology is less well-preserved and there are temporal gaps, or both. For

410 deposits <50 ka, exposure age is linearly related to distance (up to 2200 m from Law ice); r^2 for
411 ^{10}Be is ~0.8.

412 For the oldest sectors, we infer the following based on a synthesis of new and previously
413 published findings. First, farthest from the Law Glacier, sediments have been exposed close to 500
414 ka, and perhaps as long as ~1 Ma (Graly et al., 2018a). The two oldest boron-exposure ages farthest
415 from the Law Glacier in Zone 5 (southwestern sector) are ~670 ka and ~1000 ka (Figs. 2,7). We
416 assume undated ridges in the southwestern and southeastern sectors of Mt. Achenar area (Figs. 1,
417 2) are between ~500 ka and ~ 1 Ma. For the oldest Law Glacier-derived ridges in Zone 4, four
418 cosmogenic ages (one cobble-size) and two boron ages are in the ~500-400 ka range. The oldest
419 ^{10}Be - ^{26}Al sample (MAR-11-14), around 500 ka, also may be a slight underestimate for its exposure
420 duration as the discordance between the ^{26}Al and ^{10}Be ages hints that some degree of erosion and/or
421 burial modified the concentrations (Fig. 8). Our inference is consistent with Sun et al. (2015), who
422 concluded that relatively cold dry conditions have existed since the Miocene based on the
423 geochemistry of salts that are of subglacial origin near the Lewis Cliffs Ice Tongue margin.
424 Second, the Lewis Cliffs Ice Tongue expanded into the Achenar moraine system, before or close
425 to ~500 ka, given the cross-cutting relation with the dated Law moraine (yellow dashed line on
426 Fig. 2A).

427 The last ~200,000 years of the moraine history is well documented by a large number of
428 exposure ages from samples collected on quasi-continuous and often well-defined moraine ridges
429 (Fig. 2). Sediments exposed since MIS 6 and 5 are found in both the main transect and the tail
430 areas. Two ages are 135.2 ± 2.2 and 120.0 ± 2.5 , four coherent ages provide a mean of 106 ± 9.1 ka
431 (Section 4.1), and six ages cluster around 103.1 ± 8.9 ka (Section 4.2); a younger age of ~86 ka was
432 found in both the main transect and tail areas, respectively. Notably, two samples associated with

433 the ~100 ka deposits, 57.8 ± 3.0 and 39.9 ± 1.7 ka (on a cobble-size sample), overlap in age with the
434 younger moraine ridges dated from ~55 to 35 ka. Perhaps these rocks came to the surface later (see
435 Section 5.4), associated with only localized moraine disturbance around the sample location. The
436 prominent lateral moraine is 9.2 ± 0.5 ka, which overlaps with the chronology in the back of Zone
437 1 (Figs. 3, 7) and dates an early Holocene high in the Law Glacier surface.

438 The youngest exposure ages obtained from the Law Glacier surface are <100 years for two
439 cobble-sized samples and a boulder (Fig. 3). These three ^{10}Be ages, as well as other analyzed
440 samples near the tail (Fig. 5), indicate that when debris reaches the surface, it is likely to be
441 essentially free of *in situ* cosmogenic nuclides. As nuclide production occurs even before the
442 material reaches the surface, ages <100 years or a few centuries indicate minimal inheritance and
443 relative rapid upward movement (to be discussed in a future paper). Moreover, the general
444 concordance between ^{10}Be , ^3He , ^{26}Al and boron exposure ages and their progression with distance
445 from Law Glacier, also indicates there is minimal inheritance in the moraine sediments, at least
446 within the uncertainties of the three chronometers and dating of the ridges (Table 2); ~15% of the
447 samples may have some degree of complex history, based on non-concordance with the constant
448 exposure trajectory of $^{26}\text{Al}/^{10}\text{Be}$ when 1σ is considered (Fig. 8). At Mt. Achernar, a lack of pre-
449 exposure of surface material is consistent with prior studies that concluded sediment is commonly
450 sub-glacially derived, given it is faceted and striated (Bader et al., 2017; Graly et al., 2018b).

451 Several ages on cobble-size samples allows for comparison with larger boulder ages. We
452 do not find a consistent offset. Cobbles are slightly younger in some instances, although in others
453 they are the same (near modern Law ice) or older (tail). In the back of Zone 4, a cobble next to a
454 boulder is distinctly younger (500 ka versus 370 ka); although the younger cobble-size sample
455 overlaps with another nearby boulder age of ~382 ka (MAR-11-13), the older sample is consistent

456 with boron exposure ages of 500-400 kyr (Fig. 7; Graly et al., 2018a). Whether the cobble is
457 younger because it is smaller, reached the surface later, or was affected more by periglacial
458 processes compared with the larger boulder is unknown. Cobble-size samples were ≤ 5 cm thick
459 from the side facing upwards (apparent) to its bottom (Table 1), and we processed the width of the
460 sample, which should reduce effects of possible rotation; for the other two axes, cobble-size
461 samples were typically ≤ 5 cm 'wide,' except MAR-15-59 which is < 10 cm wide. The thickness
462 correction does not take into account, though, if the cobbles have complex histories of exposure
463 and burial. Although as mentioned above, cobbles that were (at least) recently exposed appear to
464 lack inherited concentrations. Additional data, including perhaps other nuclides with different half-
465 lives, are needed to decipher the precise age of the oldest deposits, and also whether the cobble-
466 sized materials typically afford younger ages than boulders.

467 A large span of the history represented in the Mt. Achnar moraine system still remains
468 unknown. Only a handful of ridges were sampled even in the main transect (Figs. 2-5). Most of
469 the ridges that are between ~ 300 ka and ~ 20 ka in age remain undated (Fig. 2). Between the MIS
470 3 (~ 55 -35 ka) and MIS 2 (19.3 ± 0.8) dated sites, there remain ~ 10 unanalyzed ridges. The
471 southwestern and southeastern sectors, which may be the oldest, and most of the tail remain
472 unsampled.

473

474 *5.2. Past central EAIS stability*

475 The Achnar moraine directly chronicles past Law Glacier behavior through its internal
476 architecture, morphology, and elevations of its current surface and lateral moraine (Fig. 3). These
477 are independent measures of either quantitative or qualitative changes in ice elevation over time.
478 Starting with internal architecture, surface sediments exposed > 10 ka (10^4 - 10^5 yr timescale) overlie

479 an estimated 140-190 m of debris-rich ice; and surface sediments exposed <10 ka overlie ~220 m
480 of relatively clean ice (Kassab et al., 2020) (Figs. 3, 9). All or most of the dated Achnar moraine
481 thus overlies glacier ice. And, the relatively cleaner ice exposed for <10 kyr (or 20 kyr?) links into
482 the trunk of Law Glacier. Ice and debris move upward, with the latter focused along debris bands
483 that are connected to the topographic highs that are moraine ridges (Figs. 3,9) (Kassab et al. 2020).
484 In this way, the Achnar site is analogous to other Antarctic blue-ice moraine sediment areas (e.g.,
485 Campbell et al., 2013; Hein et al., 2016; Akçar et al., 2020; Woodward et al. 2022).

486 An important consequence of the aforementioned structure below the moraines is that if,
487 or when, the surface of Law Glacier lowers substantially it would disturb the moraine architecture,
488 including the well-defined geomorphology and the long, mostly continuous parallel/sub-parallel
489 ridges and troughs that contain sediments exposed for 10^4 - 10^5 years (Figs. 3-5). In a scenario
490 whereby the buttressing support of Law Glacier ice is removed, it would cause surface slopes to
491 be reversed and, eventually, drawdown of the blue-ice sediment ridges. Woodward et al. (2022)
492 described such a scenario in the Heritage Range, West Antarctica, where thinning and a reversal
493 of flow occurred in a blue-ice moraine setting. Previously, based on the till characteristics and
494 provenance, Bader et al. (2017) concluded that the debris sources of the Mt. Achnar sediments
495 were relatively constant over time, which also indicates relative stability of the central EAIS.

496 Our findings, as well as those in prior studies (e.g., Scarrow et al. 2014; Bader et al., 2017)
497 raise questions including: (1) When did the preserved sediments first start to collect? (2) When
498 and how was the Mt Achnar blue-ice moraine disturbed, in ways that are recorded in its
499 geomorphology and chronology, which reflect major changes in paleoglaciology? On the first
500 question, as discussed above, we infer the oldest part of the moraine (Fig. 2) is at least 500-400 ka
501 and perhaps close to 1 Ma. Additional data are needed to evaluate further when the sediment started

502 to collect. On the second question, we infer that an important disturbance occurred when the Lewis
503 Cliffs Ice Tongue grew and impinged on the main area (Fig. 2A). Lewis Ice disturbed the Achnar
504 moraine, close to or before 500-400 ka. The timing may be before or during MIS 11 (*424,000 to*
505 *374,000 years*). With one exception, the oldest exposure ages in the back of Zone 4 are around or
506 younger than MIS 11. Moreover, we note that the 500-300 ka ages in the back of Zone 4 decrease
507 by about 10% and lie in the ~450-300 ka range (Table 2) if the LSDn scaling method (Lifton et
508 al., 2014) and a lower production rate are more appropriate for use in high latitudes and on older
509 surfaces in Antarctica (Balter et al. 2020). If correct, the findings imply slightly higher central
510 EAIS surfaces during or before MIS 11, at least associated with the Lewis Cliffs Ice Tongue. In
511 comparison, Blackburn et al. (2020) recently inferred an MIS 11 impact to the central EAIS,
512 specifically recession around the Wilkes Basin. Another disturbance to the Achnar moraine
513 morphology is recorded by the age discontinuity in the tail area, as much of a glacial cycle appears
514 missing between the grey lateral moraine and the oxidized till, which is discussed more below.

515

516 *5.3. Past Law Glacier surfaces*

517 At Mt. Achnar, the magnitude of glacier surface changes that disturb moraine
518 architecture is an outstanding question. Relatively minor surface elevation changes occurred at the
519 heads of central TAM outlet glaciers, including thinning during much of the middle-late Holocene
520 (cf., Mercer, 1968; Denton et al., 1989; Todd et al., 2010; Bromley et al., 2012; Hall et al., 2013),
521 as also documented here. At Mt. Achnar, disturbances to blue-ice moraine may depend on the
522 rate as well as the magnitude of surface elevation changes, especially relative to the subglacial
523 bedrock elevations. We infer minimal changes in the magnitude of glacier surface elevation over
524 (at least) the time periods in which dated sediments are preserved. Surface elevational changes

525 over the last ~500-400 kyr must have been minor enough to have left "intact" Zones 3 and 4 (10^4 -
526 10^5 yrs).

527 Our inferred estimates for past surface changes around the Mt. Achernar blue-ice moraine
528 are based on several observations. First, the far-maximum possible elevational drop (thinning)
529 from the current ice surface is ~150 m, which is depth of the underlying bedrock ridge (Kassab et
530 al., 2020). We conclude that such a decrease has not occurred, otherwise debris would have been
531 removed from the Mt. Achernar moraine sequence. Second, a minimum of ~50 meters of
532 widespread ice surface elevation change is needed to disturb the moraine, following Bader et al.
533 (2017). The right lateral moraine along the headwall of Mt. Achernar shown in Figure 6D-F
534 indicates ~40-50 m of thickening close to the present Law Glacier at ~10-9 ka (Bader et al., 2017).
535 We assume the right lateral moraine formed alongside the margin of a slightly expanded Law
536 Glacier, as it flowed off the plateau along Mt. Achernar. For about 0.5-1 km distance inward the
537 Achernar moraine appears relatively disturbed (see yellow lines on Fig. 6G), although some
538 semblance of moraine ridges and troughs still exist (Kassab et al., 2020). Thus, the high glacier
539 surface at ~10-9 ka and subsequent drop appears to have modified only a small area of the Achernar
540 moraine system close to the headwall. As the lateral moraine descends (southeastward) away from
541 Law Glacier and ends, the Mt. Achernar moraine regains a well-preserved ridge and trough form
542 (Fig. 6G).

543 Above the lateral moraine, a trimline (Figs. 3, 6) exists that separates material of different
544 relative weathering and indicates a higher ice surface before ~9.2 ka. We estimate that it is ~15-
545 20 m and <10 m above the lateral moraine, near MAR-15-92 and -96, respectively. These may be
546 minimum estimates given the slope and rockfall (Fig. 6 E,F). As the trimline is on a steep scree
547 slope, we did not collect samples for exposure dating. Implications of the higher, undated trimline

548 are as follows. First, if the trimline is older than or around ~500-400 ka, its age may reflect
549 thickening of Law Glacier at the same time as the Lewis Cliffs Ice Tongue expanded (Section 5.1).
550 Second, if the trimline is <500-400 ka in age, then its occurrence indicates ice surface elevations
551 may have been higher by a minimum of ~70 m (~50 m for the lateral moraine plus ~20+ m to the
552 trimline) near MAR-15-92 and ~10-20 m (i.e., above the blue-ice moraine) near MAR-15-96. If
553 the trimline is <500-400 ka in age, such increased (and then decreased) ice surface changes still
554 did not disturb more than a relatively small area (Figs. 2, 6G), and the blue-ice moraine system
555 still remained buttressed by Law Glacier.

556 A third line of evidence for relatively limited surface changes associated with preserved
557 sediments comes from the tail area, where the elevation of the oxidized sediments dated to MIS 6
558 and MIS 5 is the same as the present Law surface (Fig. 5), ~1750-1740 m. The grey-colored or
559 unoxidized moraine, dated from ~18 ka to ~1 ka, is about 5-10 m higher than the present Law
560 Glacier surface; this change, albeit possibly a minimum, did not disturb older, ≥ 100 ka deposits
561 that are only ~300 m away.

562 Fourth, changes of ≤ 30 m since MIS 2 across a widespread sector of the main area of the
563 Achnar moraine also did not disturb the older Zone 3 and 4 ridges shown in Figures 2 and 4. The
564 precise amount of current elevational change across the moraine varies depending on where
565 measured, which perhaps reflects localized processes or effects (Figs. 3, 7), such as sub-surface
566 ice behavior including relative to bedrock depth. The ~20-19 ka section of the moraine is about
567 ~20-25 m above the current Law Glacier surface, perhaps indicating higher ice input during the
568 global LGM. From ~14 to ~10 ka, there may have been relatively less ice input into the moraine
569 (Bader et al., 2017). Ice input then increased by ~9.2 ka, when the lateral moraine formed.

570 We note the net or steady rise in the moraine surface with distance from the Law Glacier,
571 shown in Figure 7. The back of Zone 4 is about 40 meters above the present ice surface, before the
572 topography declines back towards Lewis Cliffs Ice Tongue. We assume the increasing subglacial
573 bedrock elevations along with the englacial flow (Kassab et al., 2020) allow sediment-moraine
574 surface elevations to increase slightly, away from the buttressing Law Glacier. The insulation of
575 the overlying sediment, which reduces sublimation as it thickens (Lamp and Marchant, 2017), may
576 also allow slightly higher surfaces away from Law ice (Figs. 7,9).

577

578 *5.4. Blue-ice moraine processes including formation*

579 The chronology allows us to build upon prior studies at Mt. Achnar (Scarow et al., 2014;
580 Bader et al., 2017, Graly et al., 2018a,b, 2020; Kassab et al., 2020), to improve our understanding
581 of blue-ice areas and associated processes, refine conceptual models, and to raise new questions.
582 Any conceptual model needs to account for the increase in surface exposure age and till thickness
583 with distance from Law Glacier, change in sediment concentration in subsurface ice, and how new
584 sediment ridges form at the Law edge-moraine margin (Figs. 2-7, 9).

585 In the main moraine area, the debris concentration in the englacial ice is substantially
586 greater below sediment surfaces exposed longer than 50 ka, compared with younger parts of the
587 moraine (Fig. 9). Below sediment surfaces exposed >50 ka, there is a lack of distinct GPR
588 reflections; Kassab et al. (2020) hypothesized the amount of subsurface debris becomes high
589 enough that GPR reflections interfere with each other and no individual hyperbolic reflections are
590 therefore observed. In association with the large ridges, especially for those exposed ~50-35 kyr,
591 the dipping reflections appear to cluster and merge. Kassab et al (2020) inferred that underlying

592 the innermost moraine (Fig. 3, Zones 1 and 2) the lack of reflections indicates clean ice or that
593 with low debris concentration given the resolution (Fig. 9).

594 The chronology tied to the GPR-based findings lead us to infer that a significant change in
595 englacial sediment concentration occurred around or by ~50 ka, which was caused, at least in part,
596 by even earlier changes in basal entrainment (Fig. 9). For moraine exposed longer than 50 kyr, we
597 infer slower subsurface ice velocity including upward movement (Fig. 9; Kassab et al., 2020),
598 compared with that under younger parts of the moraine. Till thicknesses of ~15 cm to >1 m
599 associated with exposure ages >20 ka (Scarrow et al., 2014; Bader et al., 2017) are consistent with
600 slower rates of subsurface ice velocities. As till thickness increases, sublimation is reduced and
601 eventually may be effectively shut off (Lamp and Marchant, 2017). Sublimation helps drive ice
602 upwards (Whillans and Cassidy, 1992), hence, as its rate declines under thickening sediment
603 'horizontal' and upward ice velocities should decrease or essentially stop. In contrast, till thickness
604 <10 cm are associated with the youngest Zone 1 sediments (Bader et al., 2017), where the
605 subsurface ice is relatively clean and moraine is still forming.

606 The ^{10}Be - ^3He - ^{26}Al -Boron exposure ages allow us to refine an apparent sequential lateral
607 accretion rate, as new ridges formed at the moraine-Law Glacier margin (Kassab et al., 2020). The
608 accretion age may be similar to surface exposure age, and both may differ substantially from the
609 ice and sediment entrainment age (Fig. 9) (Graly et al., 2018b). We confirm the apparent rate of
610 debris accumulation and lateral growth has not been constant over time (Fig. 7B). The fastest
611 estimated rates of lateral accretion, >60 m/kyr, are associated with a distance of ~800-400 m from
612 the margin or roughly the ~15-5 ka exposed interval. Average rates >50 m/kyr are generally
613 characteristic of the inner 2000 m or last ~50 kyr. For moraine exposed from ~50 ka to 1 Ma, there
614 is a net decrease and then relatively constant and low apparent accretion rate, which is reflected in

615 the exponential relation between ages and distance from the margin (Fig. 7A). Additional analyses
616 are needed on ridges >50 ka to determine whether decreased apparent accretion rates reflect gaps
617 in preservation or the moraine becoming spatially compressed, or both.

618 Down flow from Mt. Achernar, the tail area records a different history than the main area
619 studied. The overall form of the tail is parallel or quasi-parallel with the current Law Glacier flow
620 direction (Figs. 1, 2A). We infer that formation of the tail has been influenced by prevailing ice
621 flow direction in a different manner than that of the main area (Fig. 1C,D). Furthermore, although
622 well-developed moraine ridges exist, particularly associated with the grey unoxidized till, they are
623 not as prominent throughout the older parts of the tail as they are in the main area (Fig. 2). Some
624 ridges in the tail are at a different orientation and appear cross-cut by the young grey moraine. In
625 addition, there is an age discontinuity in the tail area of ~60-80 kyr, which does not appear in the
626 main area. For now, we speculate a change in ice thickness occurred in relation to the subglacial
627 bed elevation, which altered the spatial pattern of debris entrainment between the tail and main
628 transect area closer to Mt. Achernar. Perhaps a shallow subglacial bedrock ridge exists between
629 the main area and the tail that shifted the accretion pattern as ice thickness changed, even by
630 relatively minor amounts. However, additional geophysical (e.g., GPR) and chronological
631 observations are needed to understand why the discontinuity exists in the downstream tail area
632 during the last glacial cycle.

633 Under particular conditions, blue-ice moraines can develop towards equilibrium forms (D.
634 Sugden personal communication). Over time, sublimation causes a progressive loss of glacier ice
635 and thickening of surface sediments, which is documented for moraine exposed for >50 ka in the
636 main at Mt. Achernar. Continued compressive glacier flow also may increase the concentration of
637 debris and perhaps ridges in older parts of the blue-ice moraine (e.g., Fig. 7). Younger samples

638 within an otherwise relatively coherent older population (Section 5.1, 'so-called outliers'), or
639 variability in exposure ages, might be expected if sublimation caused a boulder or cobble to reach
640 the surface long after (most of?) the moraine formed; resulting exposure age variability may be
641 due to active subsurface debris planes. Individual samples also may be younger because localized
642 periglacial activity caused them to move downward or rotate, and later re-emerge at the surface.
643 Our inferences are consistent with others' conclusions elsewhere in Antarctica (e.g., Fogwill et al.,
644 2012; Ackert et al. 2013; Hein et al., 2016; Woodward et al., 2022).

645

646 *5.5. Comparison with global ice sheet changes*

647 We display our results alongside the benthic $\delta^{18}\text{O}$ record, which allows comparisons
648 between exposure ages and past global climate and ice sheet changes (Lisiecki and Raymo, 2005)
649 (Fig. 10). Given that most ridges are not yet dated we highlight again, especially for older parts of
650 the Achernar moraine sequence, inferences are tentative as only parts of its history are known. The
651 findings imply slightly higher central EAIS surfaces during or before MIS 11, at least to cause
652 growth of the Lewis Cliffs Ice Tongue. Moraine ridges not yet dated may reveal an MIS 4 (cf.,
653 Doughty et al., 2021) part of the sequence. As MIS 5 ages are found both in the main and tail areas,
654 and considering the well-preserved geomorphology formed during MIS 1 (<11.8 ka), the findings
655 imply other prior interglacial periods also might be well represented in the Mt. Achernar moraine.
656 In fact, despite sampling only a small number of ridges in the main area and a small part of the
657 tail, the distributions of MIS 5 ages overlap statistically, ~105-100 ka (Lm, LSDn ages are ~10%
658 lower). Exposure ages between ~100 and 80 ka imply all MIS 5 intervals may be represented.

659 The time since MIS 2 is well documented, given sampling was comprehensive (Fig. 10).
660 There are no exposure ages overlapping with the first half of Termination I, when ice receded

661 globally (Denton et al. 2010, 2021), except for one ^{26}Al age that is high relative to its paired ^{10}Be
662 analysis (MAR-11-22). Perhaps there was less sediment delivery during peak Termination periods,
663 which is also consistent with the conclusion of Kassab et al. (2020) that colder global periods have
664 higher debris concentration and entrainment. Such changes in sediment concentration may
665 correspond to ice flow history relative to loci of entrainment, with closer sources leading to higher
666 concentrations. However, given the lack of ridges dated, such inferences need to be tested with
667 additional analyses. A high surface elevation around 9.5-9 ka is consistent with other interior EAIS
668 studies that observed thick ice during the early Holocene, perhaps associated with a lag response
669 to downstream dynamics or increased accumulation on the plateau (e.g., Hall et al., 2012).

670

671 **6. Conclusions and Questions**

672 Blue-ice moraine sediments at Mt. Achnar in the central Transantarctic Mountains offer
673 at least ~500-400 ka and likely ~1 Ma of paleoglaciologic history for the edge of the EAIS plateau.
674 Blue-ice moraines represent — for time periods in which they are preserved — relatively constant
675 EAIS outlet glacier conditions and quasi-equilibrium forms. The observations support surface
676 elevation changes associated with the Law Glacier of a minimum of ~50 m over at least the last
677 two glacial cycles. A relatively stable central EAIS occurred during MIS 5, in terms of ice surface
678 elevation, which left older MIS 6+ geomorphology and sediments intact. Our findings are
679 consistent with those of other blue-ice studies around Antarctica (e.g., Fogwill et al., 2012).
680 Disturbances to the Achnar blue-ice moraine did occur, but the magnitude of change was limited.
681 The largest obvious disturbance was when the nearby Lewis Cliffs Ice Tongue was expanded,
682 close to or prior to 500-400 ka. Gaps in the blue-ice moraine record may be more evident prior to
683 the last two glacial cycles. A slight increase in ice thickness or ice input seems associated with the

684 global LGM around ~20 ka and during the earliest Holocene, 9.2±0.5 ka. Sediments that recently
685 reached the Law Glacier surface contain negligible inheritance in the context of the older moraine
686 dating.

687 We ask the following questions specifically in terms of the Mt. Acheron record. However,
688 the answers will provide a better context and understanding of blue-ice moraines as important
689 paleoglaciological archives around Antarctica. When did sediments start to accumulate at Mt.
690 Acheron? What magnitude and rate of surface change disturbs moraine architecture, especially
691 relative to subglacial flow and bedrock elevation? What caused the Lewis Cliffs Ice Tongue to
692 expand and disturb the Law Glacier moraine sequence, and was it due to MIS 11 local climatic
693 conditions? What caused debris to increase substantially below surfaces exposed >20 ka, and
694 especially >50 ka, and are these particular times random? What determines the location of debris-
695 loaded bands or planes? We infer ridge preservation and location of debris planes may be due to
696 glacier surface history, how basal material is sub-glacially entrained, and thereafter how flow
697 occurs relative to bedrock topography and structure. Another possibility is that englacial
698 concentrations are dependent on where debris is derived, perhaps at specific places along the bed,
699 with higher amounts associated with closer sources. Future modeling-based studies can also
700 provide additional insights into blue-ice moraine processes.

701

702 **Acknowledgements**

703 This work was supported by National Science Foundation Antarctic grants PLR-
704 1443433, PLR-1443213, ANT-0944578 and ANT-0944475. We thank the Polar Geospatial
705 Center and UNAVCO (Marianne Okal, Annie Zaino, Joe Petit), the US Antarctic Program, Kenn
706 Borek Air, Ltd., Michael Roberts and Peter Braddock and all other field team members from the

707 2010/11 and 2015/16 seasons. We also thank all personnel at the Center of Accelerator Mass
708 Spectrometry (CAMS) at Lawrence Livermore National Laboratory and PRIME Lab for
709 analyses. We thank Jean Hanley and Jeremy Frisch for laboratory assistance. As Reviewers,
710 David Sugden and Peter Almond substantially improved the clarity and strength of the
711 manuscript.

712
713 **References**

- 714 Akçar, N., Yeşilyurt, S., Hippe, K., Christl, M., Vockenhuber, C., Yavuz, V., Özsoy, B., 2020.
715 Build-up and chronology of blue ice moraines in QueenMaud Land, Antarctica, Quaternary
716 Science Advances, 2, 100012.
- 717
718 Ackert, R. P., 2000. Antarctic glacial chronology: new constraints from surface exposure dating,
719 PhD thesis, Woods Hole Oceanographic Institution, Massachusetts Institute of Technology, pp.
720 213.
- 721
722 Ackert, R.P., Jr., Putnam, A.E., Mukhopadhyay, S., Pollard, D., DeConto, R.M., Kurz, M.D.,
723 Borns, H.W., Jr., 2013. Controls on interior West Antarctic Ice Sheet elevations: Inferences from
724 geologic constraints and ice sheet modeling. Quaternary Science Reviews, 65, 26–38,
725 doi:10.1016/j.quascirev.2012.12.017.
- 726
727 Bader, N.A., Licht, K.J., Kaplan, M.R., Kassab, C., Winckler, G., 2017. East Antarctic ice sheet
728 stability recorded in a high-elevation ice-cored moraine. Quaternary Science Reviews, 159, 88-
729 102.
- 730
731 Balco, G., Stone, J.O, Lifton, N.A., Dunai, T.J., 2008. A complete and easily accessible
732 means of calculating surface exposure ages or erosion rates from ^{10}Be and ^{26}Al measurements.
733 Quaternary Geochronology, 3, 174-195.
- 734
735 Balco, G., 2020. Noncosmogenic helium-3 in pyroxene and Antarctic exposure dating,
736 <https://cosmognosis.wordpress.com/2020/08/22/noncosmogenic-helium-3-in-pyroxene-and-antarctic-exposure-dating/>.
- 737
738
739 Balter-Kennedy, A., Bromley, G., Balco, G., Thomas, H., Jackson, M. S., 2020. A 14.5-million-
740 year record of East Antarctic Ice Sheet fluctuations from the central Transantarctic Mountains,
741 constrained with cosmogenic ^3He , ^{10}Be , ^{21}Ne , and ^{26}Al . The Cryosphere, 14, 2647–2672,
742 <https://doi.org/10.5194/tc-14-2647-2020>.
- 743
744 Bintanja, R., 1999. On the glaciological, meteorological and climatological significance of
745 Antarctic blue ice area. Reviews of Geophysics, 37, 337–359.
- 746

747 Blackburn, T., Edwards, G., Tulaczyk, S., Scudder, M., Piccione, G., Hallet, B., McLean, N.M.,
748 Zachos, J., Cheney, B., Babbe, J., 2020. Ice retreat in Wilkes Basin of East Antarctica during a
749 warm interglacial. *Nature*, 583, i.7817.
750
751 Borchers, B., Marrero, S., Balco, G., Caffee, M., Goehring, B., Lifton, N., Nishiizumi, K.,
752 Phillips, F., Schaefer, J., Stone, J., 2016. Geological calibration of spallation production rates in
753 the CRONUS-Earth project. *Quat. Geochronol.* 31, 188–198.
754
755 Bromley, G.R.M., Hall, B.L., Stone, J.O., Conway, H., 2012. Late Pleistocene evolution of Scott
756 Glacier, southern Transantarctic Mountains: implications for the Antarctic contribution to
757 deglacial sea level. *Quaternary Science Reviews*, 50, 1-13.
758
759 Bromley, G.R.M., Winckler, G., Schaefer, J.M., Kaplan, M.R., 2014. Pyroxene separation by HF
760 leaching and its impact on helium isotopes. *Quaternary Geochronology*, 23, 1-8.
761
762 Campbell, S., Balco, G., Todd, C., Conway, H., Huybers, K., Simmons, C., Vermeulen, M.,
763 2013. Radar-detected englacial stratigraphy in the Pensacola Mountains, Antarctica: Implications
764 for recent changes in ice flow and accumulation. *Annals of Glaciology*, 54, 91–100.
765
766 Cassidy, W., Harvey, R., Schutt, J., Disle, G., Yanai, K., 1992. The meteorite collection sites of
767 Antarctica: *Meteoritics*, v. 27, p. 490–525, doi:10.1111/j.1945-5100.1992.tb01073.x.
768
769 Chinn, T.J., 1991. Polar glacier margin and debris features. *Memorie della Societa Geologica*
770 *Italiana*, 46, 25–44.
771
772 Chinn, T.J., 1994. Glacier disequilibrium in the Convoy Range, Transantarctic Mountains,
773 Antarctica. *Institute of Geological & Nuclear Sciences Contribution*, 217, 269–276.
774
775 Corti, G., Zeoli, A., Belmaggio, P., Folco, L., 2008. Physical modeling of the influence of
776 bedrock topography and ablation on ice flow and meteorite concentration in Antarctica. *Journal*
777 *of Geophysical Research* 113(F1), doi:10.1029/2006JF000708.
778
779 DeConto, R.M., Pollard, D., 2016. Contribution of Antarctica to past and future sea-level rise.
780 *Nature*, 531, 591–597, doi:10.1038/nature17145.
781
782 Denton, G.H., Bockheim, J.G., Wilson, S.C., Leide, J.E., 1989. Late Quaternary ice surface
783 fluctuations of Beardmore Glacier, Transantarctic Mountains. *Quaternary Research* 31, 183-209.
784
785 Denton, G.H., Anderson, R.F., Toggweiler, J.R., Edwards, R.L., Schaefer, J.M., Putnam, A.E.,
786 2010. The last glacial termination. *Science* 328, 1652-1656.
787
788 Denton, G.H., Sugden, D.E., Marchant, D.R., Hall, B.L., Wilch, T.I., 1993. East Antarctic Ice
789 Sheet sensitivity to Pliocene climatic change from a Dry Valleys perspective. *Geografiska*
790 *Annaler Series A*, 75, 155-204.
791

792 Denton, G.H., Putnam, A.E., Russell, J.L., Barrell, D.J.A., Schaefer, J.M., Kaplan, M.R., Strand,
793 P.D., 2021. The Zealandia Switch: Ice age climate shifts viewed from Southern Hemisphere
794 moraines. *Quaternary Science Reviews*, 257, 106771.
795
796 Doughty, A.M., Kaplan, M.R., Peltier, C., Barker, S., 2021. A global maximum in glacier extent
797 during MIS 4. *Quaternary Science Reviews*, 261, 106948.
798
799 Eaves, S.R., Winckler, G., Schaefer, J.M., Vandergoes, M.J., Alloway, B.V., Mackintosh, A.N.,
800 Townsend, D.B., Ryan, M.T., Li, X., 2015. A test of the cosmogenic ^3He production rate in the
801 south-west Pacific (39°S). *Journal of Quaternary Science*, 30, 79-87.
802
803 Eaves, S.R., Mackintosh, A.N., Winckler, G., Schaefer, J.M., Alloway, B.V., Townsend, D.B.,
804 2016. A Cosmogenic ^3He chronology of late Quaternary glacier fluctuations in North Island,
805 New Zealand (39°S). *Quaternary Science Reviews*, 132, 40-56.
806
807 Faure, G., Mensing, T.M., Johnson, K.S., 1992. Composition of rock clasts in the Mt.
808 Achnar moraine and the Lewis Cliff ice tongue. *Antarctic Journal, U. S.* 11-12.
809
810 Fogwill, C.J., Hein, A.S., Bentley, M.J., Sugden, D.E., 2012. Do blue-ice moraines in the
811 Heritage Range show the West Antarctic ice sheet survived the last interglacial?
812 *Palaeogeography, Palaeoclimatology, Palaeoecology*, 335–336, 61–70.
813
814 Golledge, N.R. and 12 others, 2013. Glaciology and geological signature of the Last Glacial
815 Maximum Antarctic ice sheet. *Quaternary Science Reviews*, 78, 225–247.
816
817 Graly, J.A., Licht, K.J., Drushel, G.K., Kaplan, M.R., 2018a. Polar desert chronologies through
818 quantitative measurements of salt accumulation. *Geology*, 46, 351-354.
819
820 Graly, J.A., Licht, K.J., Kassab, C.M., Bird, B.W. Kaplan, M.R., 2018b. Warm-based basal
821 sediment entrainment and far-field Pleistocene origin evidenced in central Transantarctic blue ice
822 through stable isotopes and internal structures. *Journal of Glaciology* 64, 185-196.
823
824 Graly, J.A., Licht, K.J., Bader, N.A. Bish, D.L., 2020. Chemical weathering signatures from Mt.
825 Achnar Moraine, Central Transantarctic Mountains I: Subglacial sediments compared to
826 underlying rock. *Geochimica et Cosmochimica Acta*, 283, 149-166.
827
828 Hagen, E.H., 1995. A geochemical and petrological investigation of meteorite ablation products
829 in till and ice of Antarctica [Ph.D. Thesis]: Columbus, The Ohio State University, 525 p.
830
831 Hall, B.L., Denton, G.H., Stone, J.O., Conway, H., 2013. History of the Grounded Ice Sheet in
832 the Ross Sea Sector of Antarctica during the Last Glacial Maximum and the Last Termination.
833 381, Geological Society, London, pp. 167-181. Special Publication.
834
835 Hein, A., et al., 2016. Evidence for the stability of the West Antarctic Ice Sheet divide for 1.4
836 million years, *Nature Communications*, 7, 10325–10332, doi:10.1038/ncomms10325.
837

838 Higgins, J.A., Kurbatov, A.V., Spaulding, N.E., Brook, E., Introne, D.S., Chimiak, L.M., Yan,
839 Y., Mayewski, P.A., Bender, M.L., 2015. Atmospheric composition 1 million years ago from
840 blue ice in the Allan Hills, Antarctica, *Proceedings of the National Academy of Sciences*, 112
841 6887-6891.

842

843 Howat, I. M., Porter, C., Smith, B. E., Noh, M.-J., Morin, P., 2019. The Reference Elevation
844 Model of Antarctica, *The Cryosphere*, 13, 665-674, <https://doi.org/10.5194/tc-13-665-2019>.

845

846 Joy, K., Fink, D., Storey, B., Atkins, C., 2014. A 2 million year glacial chronology of the
847 Hatherton Glacier, Antarctica and implications for the size of the East Antarctic Ice Sheet at the
848 Last Glacial Maximum. *Quaternary Science Reviews*, 83, 46–57.

849

850 Kaplan, M.R., Strelin, J.A., Schaefer, J.M., Denton, G.H., Finkel, R.C., Schwartz, R., Putnam,
851 A.E., Vandergoes, M.J., Goehring, B.M., Travis, S.G., 2011. In-situ cosmogenic ¹⁰Be production
852 rate at Lago Argentino, Patagonia: Implications for late-glacial climate chronology. *Earth and*
853 *Planetary Science Letters*, 309, 21–32.

854

855 Kaplan, M.R., Licht, K.J., Winckler, G., Schaefer, J.M., Bader, N., Mathieson, C., Roberts, M.,
856 Kassab, C.M., Schwartz, R., Graly, J.A., 2017. Mid-Late Pleistocene stability of the central East
857 Antarctic Ice Sheet at the head of Law Glacier. *Geology*, 45, 963-966.

858

859 Kassab, C.M., Licht, K.J., Petersson, R., Lindbäck, K., Graly, J.A., Kaplan, M.R., 2020.
860 Formation and evolution of an extensive blue ice moraine in central Transantarctic Mountains,
861 Antarctica. *Journal of Glaciology* 66, 49-60.

862

863 Lal, D., 1991. Cosmic-ray labeling of erosion surfaces in-situ nuclide production rates and
864 erosion models. *Earth and Planetary Science Letters*, 104, 424-439.

865

866 Lamp, J.L., Marchant, D.R., 2017. Vapor transport and sublimation on Mullins Glacier,
867 Antarctica. *Earth and Planetary Science Letters* 465, 82-91.

868

869 Lisiecki, L.E., Raymo, M.E., 2005. A Pliocene-Pleistocene stack of 57 globally distributed
870 benthic delta O-18 records. *Paleoceanography* 20.

871

872 Lifton, N., Sato, T., Dunai, T., 2014. Scaling in situ cosmogenic nuclide production rates using
873 analytical approximations to atmospheric cosmic-ray fluxes. *Earth and Planetary Science Letters*
874 386 149-160.

875

876 Mercer, J.H., 1968. Glacial geology of the Reedy glacier area, Antarctica. *Geological Society of*
877 *America Bulletin*, 79, 471-486.

878

879 Palmer, E.F., Licht, K.J., Swope, R.J., Hemming, S.R., 2012. Nunatak moraines as a repository
880 of what lies beneath the East Antarctic ice sheet. In: Rasbury, E.T., Hemming, S.R., Riggs, N.R.
881 (Eds.), *Mineralogical and Geochemical Approaches to Provenance*, 487. *Geological Society of*
882 *America Special Paper*, pp. 97-104.

883

884 Pattyn, R. 2010. Antarctic subglacial conditions inferred from a hybrid ice sheet/ice stream
885 model. *Earth and Planetary Science Letters* 295, 451–461.
886

887 Putnam, A., Schaefer, J., Barrell, D.J.A., Vandergoes, M., Denton, G.H., Kaplan, M., Finkel,
888 R.C., Schwartz, R., Goehring, B.M., Kelley, S., 2010. In situ cosmogenic ¹⁰Be production-rate
889 calibration from the Southern Alps, New Zealand. *Journal of Quaternary Geochronology*, 5,
890 392–409.
891

892 Scarrow, J.W., Balks, M.R., Almond, P.C., 2014. Three soil chronosequences in recessional
893 glacial deposits near the polar plateau, in the Central Transantarctic Mountains, Antarctica.
894 *Antarctic Science* 26, 573-583.
895

896 Schäfer, J. M., S. Ivy-Ochs, R. Wieler, I. Leya, H. Baur, G. H. Denton, C. Schlüchter, 1999.
897 Cosmogenic noble gas studies in the oldest landscape on earth: surface exposure ages of the Dry
898 Valleys, Antarctica. *Earth and Planetary Science Letters*, 167, 215-226.
899

900 Schaefer, J.M., Denton, G.D., Kaplan, M.R., Putnam, A., Finkel, R.C., Barrell, D.J.A., Andersen,
901 B.G., Schwartz, R., Mackintosh, A., Chinn, T., Schlüchter, C., 2009. High frequency Holocene
902 glacier fluctuations in New Zealand differ from the northern signature. *Science* 324, 622–625.
903

904 Sinisalo, A., Moore, J.C., 2010. Antarctic blue ice areas – towards extracting paleoclimate
905 information. *Antarctic Science*, 22, 99–115.
906

907 Stone, J.O., 2000. Air pressure and cosmogenic isotope production. *Journal Geophysical*
908 *Research*, 105, 23753-23759.
909

910 Sun, T., Socki, R.A., Bish, D.L., Harvey, R.P., Bao, H., Niles, P.B., Cavicchioli, R., and Tonui,
911 E., 2015. Lost cold Antarctic deserts inferred from unusual sulfate formation and isotope
912 signatures. *Nature Communications*, 6, 7579, doi:10.1038/ncomms8579.
913

914 Todd, C., Stone, J. O. H., Conway, H., Hall, B., Bromley, G., 2010. Late Quaternary evolution of
915 Reedy Glacier, Antarctica. *Quaternary Science Reviews*, 29, 1328–1341.
916

917 Westoby, M.J., Dunning, S.A., Woodward, J., Hein, A.S., Marrero, S.M., Winter, K., Sugden,
918 D.E., 2016. Interannual surface evolution of an Antarctic blue-ice moraine using multi-temporal
919 DEMs. *Earth Surface Dynamics*, 4, 515-529.
920

921 Whillans, I.M., Cassidy, W.A., 1983. Catch a falling star: Meteorites and old ice. *Science*, 222,
922 55–57, doi:10.1126/science.222.4619.55.
923

924 Whitehouse, P.L., Bentley, M.J., Le Brocq, A.M. 2012. A deglacial model for Antarctica:
925 geological constraints and glaciological modelling as a basis for a new model of Antarctic glacial
926 isostatic adjustment. *Quaternary Science Reviews* 32, 1–24.
927

928 Woodward, J., Hein, A., Winter, K., Westoby, M., Marrero, S., Dunning, S., Lim, M., Rivera, A.
929 Sugden, D., 2022. Blue-ice moraines formation in the Heritage Range, West Antarctica:

930 Implications for ice sheet history and climate reconstruction., *Quaternary Science Advances*, 6,
931 100051.

932
933

934 **Figure Captions.**

935
936 Figure 1. Setting of the Mt. Acheron area. A) Mt. Acheron moraine sits at the head of Law Glacier

937 (within red box) where unconstrained flow off of the East Antarctic plateau becomes constrained

938 through Transantarctic Mountains. B) Ice surface velocities and sediment catchment area for the

939 Mt. Acheron area (Bader et al. 2017; Graly et al., 2018b). C) The entire moraine complex along

940 with locations of sediment (till) samples for study of provenance changes (Bader et al., 2017) and

941 soil geochemistry (Graly et al., 2017). Also shown are zones (in white) defined in Bader et al.

942 (2017), the general area of study by Scarrow et al. (2014), and ice flow directions with arrows.

943 Note the ice flow is steered away from the main trunk glacier, where it is then trapped in the

944 embayment (Kassab et al. 2020). D) Image of the Acheron moraine and surrounding area, from

945 Antarctic REMA (Reference Elevation Model of Antarctica) Explorer (Howat et al., 2019).

946

947 Figure 2. All ^{10}Be - ^{26}Al - ^3He ages obtained in the Mt. Acheron area. A) The study area including

948 the tail area (NW sector), which is shown in more detail in Figure 5. The yellow-dashed line

949 outlines moraine associated with the Lewis Cliffs Ice Tongue, which impinged on and disturbed

950 the Mt. Acheron blue-ice moraine. We show the two oldest boron-exposure ages (Graly et al.,

951 2018a) (Fig. 1C), in the southwestern sector, to the right of Lewis Cliffs Ice Tongue. B) A focus

952 on the main and lateral moraine areas, which are shown in more detail in Figures 3 and 4. Italicized

953 ages are discussed as outliers. All exposure ages are on boulders except those labelled 'c' (cobble-

954 size). All ages in ka, except for three ^{10}Be ages in pink (years), which are on samples from the

955 Law Glacier margin (see next, Figure 3 for more detail). Yellow-dashed lines with associated ages
956 mark approximate age boundaries.

957

958 Figure 3. Focus on the best-dated Zones 1 and 2, looking west with the Law Glacier on the right.
959 Headwall of Mt. Achernar shown in background. Four ^{10}Be ages on samples along the lateral
960 moraine, date to 9.2 ± 0.5 ka and record a high surface for ice flowing off the plateau, which is
961 seen in the upper right. GPR radargram profile below the photo is from Kassab et al. (2020), and
962 more or less follows the yellow-dashed line. Dipping stacked and scattered hyperbolas are
963 inferred to represent planes of debris and cobbles/boulders causing point reflectors, respectively.
964 Figure 6 provides additional photos of the lateral moraine with samples.

965

966 Figure 4. Similar to Figure 3, with photos focusing on Zones 2 to 4 and cosmogenic exposure ages.
967 Top panel focuses on Zone 2, with the Law Glacier (Fig. 3) on right side. Middle panel focuses on
968 Zones 2 and 3 including moraines dated to MIS 2 time; the average and standard deviation are
969 19.3 ± 0.8 ka excluding the one outlier of 5.9 ± 0.1 . Bottom panel focuses on inner Zone 4 and
970 samples dating to <100 ka. Mt Achernar headwall is in the background. In each subsequent panel,
971 some overlap in exposure ages is shown on right side.

972

973 Figure 5. A focus on the tail area, with view looking southwest, towards Mt. Achernar. Law Glacier
974 is on the right. Note relatively oxidized sediments on the left side of the photo, which date to MIS
975 6 and 5 except for 1 outlier of ~ 18.6 ka. Also shown are MIS 5 ages (~ 135.2 to ~ 86.1 ka) from the
976 main area of focus (Fig. 2B), which is in the background. All are boulder ages except if labelled
977 "c" (cobble size). Two outliers are italicized. See Figure 6 for photos that focus on the right side

978 of image; both the ~0.3 and ~0.9 ka ages are slightly closer to the present margin, compared with
979 the ~1.1 and ~2.7 ka ages.

980

981 Figure 6. Photos that provide context of geomorphology and age data. A) Three ^{10}Be ages near
982 the moraine/ Law Glacier boundary. Person for scale. In this panel the three ages are in years, in
983 all other panels they are in ka. B) and C) A focus on the tail area and samples MAR-15-87 (ice
984 margin) and -88 (+4 m). D) The lateral moraine, with two apparent ridges. E) The lateral
985 moraine and trimline, close to (NW of) sample MAR-15-92c (panel G). The tallest boulders are
986 ~1 m in height and we estimate the trimline is about 15-20 m higher. F) The lateral moraine and
987 trimline, by MAR-15-98c (panel G). We estimate the trimline is <10 m higher. G) The area near
988 the lateral moraine with ^{10}Be ages (all cobbles). We also show the elevation difference between
989 the Law Glacier (1858 m), lateral moraine (~1905 m), and towards the south (1868 m). Note the
990 area next to the lateral moraine is smoother without distinct ridges, as exists to the left (east)
991 closer to the area of the main transect (white-dashed line, Fig. 2). We infer disturbances within
992 ~500 m of the lateral moraine due to the rise in surface by ~10-9 ka and when the trimline
993 formed.

994

995 Figure 7. ^{10}Be - ^3He -Boron exposure ages with distance from the Law Glacier along the main
996 transect (white-dashed line, Fig. 2). **Panels A, B)** Left side is plotted as log-log plot. Three
997 respective exponential relations demonstrate there is a steady increase in age from the active
998 margin. Within ~2200 m (~50 ka) from the Law Glacier, if the relation is represented by a linear
999 line, the r^2 is ~0.8 (^{10}Be) or ~0.6 (^3He). Boron ages are from Graly et al. (2018a). Circle marks
1000 younger sediment dated, where ^{10}Be - ^{26}Al -Boron exposure ages all indicate exposure for less time.

1001 In panel B, approximate average accretion rate based on ^{10}Be and the two oldest Boron ages at
1002 ~5600-6100 m. **Panels C, D**) Topographic profiles from Bader et al. (2017) and Kaplan et al.
1003 (2017). In panel C, the ages from Hagen (1995) are at the bottom because it is not clear how they
1004 align with the main transect. MIS labels are approximately located with distance. For simplicity,
1005 ^{26}Al ages are not shown. In Panel D, Zones 1 to 3 (Z1-Z3) are shown along bottom.

1006

1007 Figure 8. Plot of $^{26}\text{Al}/^{10}\text{Be}$ ratios versus ^{10}Be concentrations, with data colored in blue and red
1008 from Hagen (1995) and Kaplan et al. (2017), respectively, recalculated with updated systematics.
1009 MAR-11-22 is not shown on the plot due to its high $^{26}\text{Al}/^{10}\text{Be}$ value (Table 1). The first and last
1010 parts of each sample name are shown next to analyses. The ratios are standardized (*) to 6.75, the
1011 Be-10 concentrations are relative to 07KNSTD and sea level high latitude (Balco et al., 2008).
1012 Error bars are 1σ analytical uncertainty.

1013

1014 Figure 9. Ground Penetrating radar (GPR, 25MHz) with approximate locations of ^{10}Be - ^3He above
1015 the topographically corrected surface. Ages are shifted slightly so as to be at their approximate
1016 location along GPR transect. The upper panel is the processed radargram and the lower panel has
1017 interpretations including red-dashed lines as debris planes. Kassab et al. (2020) interpreted the
1018 blue-dashed line, which represents a continuous subhorizontal reflector, to be the bedrock surface
1019 at ~140 m to >220 m below. Above the GPR data, we show both maximum sediment entrainment
1020 age (Graly et al., 2020, Kassab et al. 2020) and surface exposure ages. Boundaries between MIS
1021 are fuzzy given ranges of ages. Kassab et al. (2020) also presented GPR analyses for inner Zone
1022 4, with exposure ages $\geq 100\text{ka}$, but they found a lack of consistent GPR reflections. For simplicity,
1023 ^{26}Al ages are not shown.

1024

1025 Figure 10. ^{10}Be - ^{26}Al - ^3He ages compared with benthic $\delta^{18}\text{O}$ stack (Lisiecki and Raymo, 2004). Top
1026 panels include ages with St/Lm scaling (difference not discernable at the scale shown). During
1027 MIS 5, a concentration of ages occurs at 120-100 ka excluding "outlier" ages <90 ka from the same
1028 sites (Fig. 5). Taken at face value these ages overlap with MIS5c or 5c-d. Bottom panels include
1029 exposure ages calculated with the LSDn scaling (Table 1,3) method, which are ~10-12% lower
1030 than those calculated using St/Lm.

1031

1032

Table 1. Geographical and Analytical details for ^{10}Be and ^{26}Al samples

Sample ID	Latitude (DD)	Longitude (DD)	Elevation (m)	Sample Thickness (cm)	Shielding correction	Quartz weight (g)	Carrier (Be) Added (g)	$^{10}\text{Be}/^{9}\text{Be} \pm 1\sigma$	$^{26}\text{Al}/^{27}\text{Al} \pm 1\sigma$	Total Al	$^{26}\text{Al} \pm 1\sigma$ (atoms g^{-1})	$^{26}\text{Al}/^{10}\text{Be} \pm 1\sigma$
MAR-11-22	-84.1866	161.2649	1823.14	0.61	0.999	3.0517	0.1868	8.2943E-14 ± 1.8425E-15	2.2501E-13 ± 1.7538E-14	1.9849	3.2401E+06 ± 2.5254E+05	9.6
MAR-11-10	-84.2216	161.3567	1847.24	1.07	1.000	10.5039	0.1870	3.6375E-12 ± 5.2707E-14	1.3026E-11 ± 2.3824E-13	1.0860	3.1280E+07 ± 5.7209E+05	6.9
MAR-11-18	-84.1906	161.2829	1825.41	1.05	0.999	16.8605	0.1874	1.4726E-13 ± 2.7890E-15	3.1385E-13 ± 2.3831E-14	1.9681	9.0289E+05 ± 6.8557E+04	7.4
MAR-11-26	-84.2086	161.3498	1837.80	1.67	1.000	6.8121	0.1873	3.4409E-12 ± 4.8423E-14	7.9704E-12 ± 2.0844E-13	1.7343	3.0733E+07 ± 8.0373E+05	7.2
MAR-11-30	-84.198	161.2619	1836.72	1.07	0.997	7.1486	0.1881	8.5767E-13 ± 2.0059E-14	2.2938E-12 ± 5.5104E-14	1.4846	8.8623E+06 ± 2.0517E+05	7.0
MAR-11-37	-84.2008	161.3199	1832.74	1.36	0.999	10.0921	0.1871	2.0833E-12 ± 2.5791E-14	4.2631E-12 ± 8.2534E-14	1.8284	1.7165E+07 ± 3.3232E+05	6.9
BLANK_1_2012May01							0.1846	3.1379E-16 ± 1.0460E-16	3.6006E-15	1.0131		
BLANK_2_2012May01							0.1859	3.3032E-16 ± 1.1144E-16	3.6006E-15	1.6752		
MAR-11-14a	-84.2194	161.3374	1845.51	2.02	1.000	4.0553	0.1838	3.9103E-12 ± 4.2992E-14	7.2650E-12 ± 1.3529E-13	1.6752	6.6932E+07 ± 1.2464E+06	5.7
MAR-11-14b	-84.2194	161.3374	1845.51	3.02	1.000	4.0632	0.1852	3.8754E-12 ± 4.2663E-14	7.3518E-12 ± 1.3708E-13	1.6917	6.8267E+07 ± 1.2729E+06	5.8
MAR-11-17	-84.1907	161.282	1825.76	1.10	0.999	5.0766	0.1875	6.4713E-14 ± 1.7348E-15	1.8906E-13 ± 1.9192E-14	1.2010	9.5426E+05 ± 9.6869E+04	6.2
MAR-11-33	-84.197	161.2506	1836.37	1.87	0.999	8.0920	0.1868	5.9276E-13 ± 7.6799E-15	1.3267E-12 ± 4.4710E-14	1.5731	5.7292E+06 ± 1.9308E+05	6.3
Blank_2_2013Jan24							0.1833	2.1064E-15 ± 7.0963E-16	6.9381E-15 ± 4.9072E-15	1.4472		
MAR-15-63	-84.1815	161.2797	1805.76	2.02	0.99	71.3604	0.1881	1.2475E-14 ± 6.0648E-16	1.8808E-01 ± 1.2572E+19			
MAR-15-89	-84.1011	162.13	1726.54	2.90	0.99	68.2679	0.1894	1.8575E-12 ± 2.2053E-14	1.8942E-01 ± 1.2662E+19			
BLK1-2017Jan20							0.1901	7.4243E-16 ± 2.6619E-16	1.9015E-01 ± 1.2710E+19			
BLK2-2017Jan20							0.1894	2.1044E-15 ± 6.0420E-16	1.8942E-01 ± 1.2662E+19			
MAR-15-57	-84.1869	161.2382	1825.56	1.30	0.99	5.0465	0.2094	1.0989E-13 ± 2.1170E-15	2.1095E-01 ± 1.4100E+19			
MAR-15-58	-84.1869	161.2344	1822.93	1.15	0.99	5.1301	0.2102	9.8471E-14 ± 1.8819E-15	2.1022E-01 ± 1.4052E+19			
MAR-15-59	-84.1851	161.2603	1821.98	4.25	0.99	9.1888	0.2108	9.5336E-14 ± 1.7955E-15	2.1084E-01 ± 1.4093E+19			
BLK1-2017Mar31							0.2108	8.3073E-16 ± 2.2658E-16	2.1084E-01 ± 1.4093E+19			
BLK2-2017Mar31							0.2111	1.0428E-15 ± 2.4995E-16	2.1105E-01 ± 1.4107E+19			
MAR-15-62	-84.183	161.2835	1811.08	1.16	0.99	11.8519	0.2112	8.6337E-14 ± 2.4524E-15	2.1116E-01 ± 1.4114E+19			
MAR-15-107	-84.1828	161.2698	1823.27	1.79	0.99	10.0178	0.2111	5.8470E-14 ± 1.5704E-15	2.1105E-01 ± 1.4107E+19			
MAR-15-108	-84.1826	161.2707	1823.27	1.48	0.99	10.0021	0.2107	5.3998E-14 ± 1.5487E-15	2.1074E-01 ± 1.4086E+19			
BLK3-2017Mar31							0.2109	6.5596E-15 ± 5.1785E-16	2.1095E-01 ± 1.4100E+19			
BLK4-2017Mar31							0.2109	5.7627E-16 ± 1.4250E-16	2.1095E-01 ± 1.4100E+19			
MAR-15-101	-84.187	161.2673	1819.72	0.88	0.99	5.0128	0.2112	8.1879E-14 ± 1.8060E-15	2.1119E-01 ± 1.4116E+19			
MAR-15-102	-84.1887	161.2869	1824.17	1.45	0.99	5.0146	0.2106	1.2888E-13 ± 2.4900E-15	2.1087E-01 ± 1.4075E+19			
MAR-15-105	-84.1872	161.2756	1819.72	1.14	0.99	5.0264	0.2116	1.0568E-13 ± 2.4496E-15	2.1161E-01 ± 1.4144E+19			
MAR-15-110	-84.1823	161.2723	1823.27	1.56	0.99	10.264	0.2117	1.1291E-14 ± 5.7741E-16	2.1171E-01 ± 1.4151E+19			
BLK-2017Apr24							0.2115	5.5490E-16 ± 1.4507E-16	2.1150E-01 ± 1.4137E+19			
MAR-15-123	-84.2057	161.3475	1843	1.93	0.99	5.0634	0.2110	7.6295E-13 ± 1.1594E-14	2.1098E-01 ± 1.4103E+19			
MAR-15-124	-84.2056	161.3488	1848	0.99	0.99	5.0628	0.2113	1.0646E-12 ± 2.1445E-14	2.1129E-01 ± 1.4123E+19			
MAR-15-127	-84.193	161.0739	1867.90	3.58	0.99	5.0203	0.2118	1.6935E-13 ± 3.2120E-15	2.1181E-01 ± 1.4158E+19			
MAR-15-129	-84.1928	161.2845	1826.45	0.51	0.99	5.1102	0.2116	5.4337E-14 ± 1.2848E-15	2.1161E-01 ± 1.4144E+19			
MAR-15-130	-84.193	161.2735	1831.73	0.97	0.99	5.2448	0.2115	1.7745E-13 ± 3.2912E-15	2.1150E-01 ± 1.4137E+19			
MAR-15-61*	-84.1852	161.2618	1821.98	3.55	0.99	2.2905	0.2108	1.1178E-14 ± 2.6466E-15	2.1075E-01 ± 1.4087E+19			
MAR-15-92*	-84.1783	160.988	1904.60	4.00	0.96	2.6515	0.2113	4.0871E-14 ± 2.2903E-15	2.1127E-01 ± 1.4122E+19			
MAR-15-96*	-84.193	161.0739	1867.90	3.58	0.97	3.8038	0.2109	6.3878E-14 ± 4.0279E-15	2.1086E-01 ± 1.4094E+19			
MAR-15-113*	-84.2194	161.3371	1845.51	2.03	0.99	2.4022	0.2110	1.4587E-12 ± 2.4562E-14	2.1096E-01 ± 1.4101E+19			
MAR-15-115*	-84.1185	161.905	1744.06	1.38	0.99	5.1354	0.2109	8.9057E-13 ± 1.8826E-14	2.1086E-01 ± 1.4094E+19			
MAR-15-116*	-84.1185	161.9035	1744.06	0.97	0.99	5.1346	0.2108	8.8475E-13 ± 2.5301E-14	2.1075E-01 ± 1.4087E+19			
MAR-15-117*	-84.12	161.8898	1740.26	1.37	0.99	5.0444	0.2101	8.4521E-13 ± 1.9706E-14	2.1013E-01 ± 1.4046E+19			
MAR-15-118*	-84.1201	161.8926	1740.26	2.2	0.99	5.5238	0.2104	1.6919E-13 ± 5.6893E-15	2.1044E-01 ± 1.4067E+19			
BLK-2017May10							0.2111	1.7418E-16 ± 2.5100E-16	2.1107E-01 ± 1.4108E+19			
MAR-15-121*	-84.1185	161.9035	1744.06	4.58	0.99	5.0141	0.2105	6.8561E-13 ± 1.2952E-14	2.1055E-01 ± 1.4100E+19			

MAR-15-64	-84.1814	161.2815	1807.76	5.17	1.00	60.2190	0.1881	6.6579E-15	1.2708E-13	1.2570E+19
MAR-15-65	-84.145	161.6559	1807.76	5.03	1.00	60.3486	0.1889	9.5706E-15	4.0044E-14	1.2620E+19
MAR-15-111	-84.1818	161.2609	1822	5.42	1.00	59.0633	0.1894	1.1843E-13	2.0394E-14	1.2607E+19
Bk1-2018Apr12							0.1882	6.9705E-16	1.8045E-13	1.2577E+19
MAR-15-142-T	-84.108	162.0283	1735.46	1.2	1.00	25.1410	0.1884	1.2708E-13	2.9053E-15	1.2593E+19
MAR-15-143	-84.1079	162.0362	1735.53	2.17	1.00	25.0331	0.1888	4.0044E-14	9.7898E-16	1.2621E+19
MAR-15-139	-84.1784	161.546	1765.28	2.23	1.00	15.0371	0.1886	2.2616E-14	7.7663E-16	1.2607E+19
MAR-15-142-H	-84.1793	161.5309	1762.27	1.47	1.00	15.0697	0.1888	2.0394E-14	8.0085E-16	1.2621E+19
MAR-15-145	-84.1711	161.6566	1753.73	1.11	1.00	15.3124	0.1886	1.8045E-13	3.3488E-15	1.2607E+19
Bk1-2018May02							0.1886	4.5315E-16	1.4450E-16	1.2607E+19
MAR-15-132	-84.1016	162.1294	1734.24	1.91	1.00	15.6711	0.1886	2.1908E-14	9.8354E-16	1.2607E+19
MAR-15-133	-84.1016	162.1297	1733.24	2.39	1.00	4.0390	0.1886	1.2773E-14	5.6459E-16	1.2607E+19
MAR-15-137	-84.0944	162.2205	1736	2.41	1.00	25.0135	0.1876	8.2752E-13	1.3800E-14	1.2538E+19
MAR-15-94	-84.1826	161.0115	1894.53	4.22	0.96	25.2107	0.1889	4.7329E-13	5.9377E-15	1.2638E+19
MAR-15-97	-84.1928	161.0732	1867.90	3.45	0.97	19.7066	0.1887	3.4883E-13	5.9739E-15	1.2614E+19
BLK2-2018May02							0.1879	3.5369E-16	1.1799E-16	1.2558E+19
MAR-15-76	-84.1401	161.6932	1743.05	5.13	<i>average</i>			1.3124E-16		
MAR-15-87	-84.1068	162.0493	1731.42	5.00	1.00	68.8982	0.1858	7.0104E-15	3.9843E-16	1.2420E+19
MAR-15-88	-84.1414	161.6911	1760	4.29	1.00	71.2908	0.1858	4.2733E-14	1.3147E-15	1.2420E+19
BLK1-2019Jan31					1.00	70.6214	0.1858	1.4030E-13	2.5992E-15	1.2420E+19
BLK2-2019Jan31							0.1856	1.1055E-15	2.1689E-16	1.2406E+19
					<i>average</i>		0.1853	7.8632E-16	1.7585E-16	1.2385E+19
										1.9637E-16

1035

1036

1037

1038

1039

1040

1041

1042

1043

Notes: The first two sets of samples (n=10) above the horizontal black line are from Kaplan et al. (2017). Samples with asterisk – associated with blank BLK2017May10 – were analyzed at PRIME Lab, all others were analyzed at CAMS-LLNL. Given large uncertainty for MAR-15-61 (>20%), it is not used. Sample elevations to a whole number were measured with a handheld GPS, otherwise by differential GPS (Trimble). AMS standard used for normalization is 2.85x10⁻¹²=07KNSTD3110. Shown are 1σ analytical AMS uncertainties. Column of ⁹Be added is adjusted for carrier (Be) concentration. Tables also are provided as Supplementary Material.

Table 2. Surface-exposure sample details and ³He data.

Sample ID	Latitude (DD)	Longitude (DD)	Elevation (masl) ^a	Sample Thickness (cm)	Shielding correction	Pyroxene Mass (g)	He ³ /He ⁴ ± 1σ	[³ He] ± 1σ (atoms/g)	standard
MAR-11-08	-84.1910	161.2749	1829.79	1.07	0.999	0.0719	7.4858E+05 ± 8.690E-08	9.215E+06 ± 7.486E+05	MM
MAR-11-08						0.0312	8.7819E+05 ± 1.136E-07	1.073E+07 ± 8.782E+05	MM
MAR-11-08 avg								9.973E+06 ± 8.160E+05	
MAR-11-23	-84.1870	161.2414	1825.85	1.35	0.999	0.0460	1.0899E-07 ± 8.539E-09	8.317E+06 ± 5.385E+05	MM
MAR-11-23						0.0371	1.3302E-07 ± 9.684E-09	9.397E+06 ± 6.839E+05	MM
MAR-11-23 avg								8.857E+06 ± 6.155E+05	
MAR-11-52	-84.2286	161.2652	1830.53	1.09	0.999	0.0516	5.5264E+06 ± 9.438E-06	2.380E+08 ± 5.526E+06	MM
MAR-11-48Green	-84.2268	161.2755	1840.52	1.13	0.999	0.0254	2.2413E+06 ± 2.363E-06	8.237E+07 ± 2.241E+06	MM
MAR-11-48Red	-84.2268	161.2755	1840.52	1.13	0.999	0.0263	2.2742E+06 ± 3.169E-07	8.281E+07 ± 2.274E+06	MM
MAR-11-21AL	-84.1887	161.2672	1823.14	1.09	0.999	0.0285	9.4099E+05 ± 3.169E-07	1.769E+06 ± 9.410E+05	MM
MAR-11-21CM	-84.1887	161.2672	1823.14	1.09	0.999	0.0333	8.1605E+05 ± 2.744E-07	1.557E+07 ± 8.161E+05	MM
MAR-11-35	-84.2011	161.3220	1827.24	1.31	0.999	0.0315	1.9503E+06 ± 1.271E-06	7.354E+07 ± 1.950E+06	MM
MAR-11-01	-84.1790	161.5365	1765.28	1.29	0.999	0.0290	4.4749E+05 ± 6.990E-08	5.029E+06 ± 4.475E+05	MM
MAR-11-02	-84.1791	161.5366	1765.28	0.57	0.999	0.0227	5.5215E+05 ± 1.040E-07	5.076E+06 ± 5.522E+05	MM
MAR-11-09	-84.1911	161.2725	1829.28	1.00	0.999	0.0262	5.9883E+05 ± 1.093E-07	8.530E+06 ± 5.988E+05	MM
MAR-15-112	-84.1414	161.6911	1822	3.87	0.998	0.1250	4.1334E-08 ± 1.328E-09	1.296E+07 ± 4.063E+05	Air
MAR-15-112						0.1226	4.2506E-08 ± 1.125E-09	1.333E+07 ± 3.457E+05	Air
MAR-15-112_avg								1.315E+07 ± 3.772E+05	
MAR_15_120	-84.1190	161.8995	1744.06	1.68	0.990	0.2001	4.6848E-06 ± 7.864E-08	7.219E+07 ± 1.187E+06	MM
MAR_11_41	-84.1087	162.0593	1737.80	0.94	0.990	0.2002	6.0928E-07 ± 9.308E-09	1.096E+08 ± 1.444E+06	Air
MAR_11_42	-84.1087	162.0578	1737.80	1.10	0.990	0.2002	2.1186E-07 ± 3.354E-09	7.842E+07 ± 1.081E+06	Air
MAR_15_126	-84.2060	161.3452	1847	1.00	0.990	0.1993	9.8634E-07 ± 1.485E-08	1.360E+08 ± 1.761E+06	Air
MAR_15_119	-84.1198	161.8960	1740.26	1.06	0.990	0.5028	1.1002E-06 ± 1.638E-08	7.050E+07 ± 9.003E+05	Air
MAR_15_125_2	-84.2056	161.3483	1860	2.30	0.990	0.5008	3.1158E-06 ± 4.583E-08	1.021E+08 ± 1.281E+06	Air
MAR_15_128_2	-84.1930	161.2859	1826.45	2.16	0.990	0.5033	2.9126E-07 ± 4.954E-09	1.374E+07 ± 2.090E+05	Air
MAR_15_131_2	-84.1930	161.2720	1831.73	0.99	0.990	0.4975	3.4440E-07 ± 5.719E-09	1.533E+07 ± 2.264E+05	Air
MAR_11_13	-84.2209	161.3382	1847.94	1.09	0.990	0.2018	1.0618E-06 ± 1.556E-08	2.889E+08 ± 3.610E+06	Air
MAR_11_15	-84.2190	161.3443	1846.23	2.15	0.990	0.2000	7.3744E-07 ± 1.103E-08	1.673E+08 ± 2.146E+06	Air
MAR_11_43	-84.1082	162.0607	1744.17	1.07	0.990	0.2016	1.0482E-06 ± 1.611E-08	9.634E+07 ± 1.283E+06	Air
MAR_15_122_2	-84.1185	161.9035	1744.06	3.75	0.990	0.0731	1.3895E-07 ± 2.485E-09	7.891E+07 ± 1.271E+06	Air
MAR-11-25	-84.2087	161.3480	1837.80	1.74	0.999	0.0111	2.2807E-07 ± 1.097E-08	5.633E+07 ± 2.425E+06	MM
MAR-11-25b	-84.2087	161.3480	1837.80	1.74	0.999	0.0193	2.3889E-07 ± 2.213E-08	5.503E+07 ± 3.936E+06	MM
MAR-11-25b						0.0106	2.2388E-07 ± 1.097E-08	5.444E+07 ± 2.399E+06	MM
MAR-11-25b avg								5.473E+07 ± 3.260E+06	
MAR-11-27	-84.2085	161.3655	1836.56	1.09	0.999	0.0106	8.9096E-07 ± 3.425E-08	1.498E+08 ± 4.803E+06	MM
MAR-11-28	-84.2082	161.3619	1836.77	2.17	0.999	0.0000	5.9706E-07 ± 1.2397E-08	1.675E+08 ± 3.455E+06	Air
MAR-11-29	-84.1980	161.2660	1835.95	1.58	0.999	0.0247	2.9678E-07 ± 1.787E-08	4.544E+07 ± 2.217E+06	MM
MAR-11-29							3.1097E-07 ± 1.570E-08	4.498E+07 ± 2.062E+06	MM
MAR-11-29 avg								4.521E+07 ± 2.141E+06	MM
MAR-11-31	-84.1977	161.2584	1837.49	1.11	0.999	0.0257	2.7176E-07 ± 1.701E-08	2.463E+07 ± 1.503E+06	MM
MAR-11-31							2.2397E-07 ± 1.445E-08	3.307E+07 ± 1.702E+06	MM
MAR-11-31 avg								2.885E+07 ± 1.605E+06	
MAR-11-32	-84.1970	161.2508	1836.37	1.90	0.999	0.1144	3.8387E-08 ± 1.267E+07	1.267E+07 ± 5.055E+05	Air
MAR-11-34	-84.1971	161.2372	1836.37	1.29	0.999	0.0117	1.7393E-07 ± 9.307E-09	3.884E+07 ± 1.908E+06	MM
MAR-11-36	-84.2008	161.3194	1832.74	0.83	0.999	0.0181	3.7043E-07 ± 2.329E-08	4.271E+07 ± 2.227E+06	MM
MAR-11-36							3.8036E-07 ± 2.073E-08	4.473E+07 ± 2.255E+06	MM
MAR-11-36 avg								4.372E+07 ± 2.241E+06	
MAR-11-38	-84.2006	161.3078	1826.12	0.84	0.999	0.0925	2.3212E-07 ± 5.2394E-09	9.406E+07 ± 2.112E+06	Air
MAR-11-39	-84.2006	161.3019	1827.10	0.97	0.999	0.1158	3.7897E-07 ± 0.000E+00	1.021E+08 ± 2.255E+06	Air
MAR-11-40	-84.2006	161.3019	1827.10	2.32	0.999	0.0254	5.8912E-07 ± 2.757E-08	2.965E+07 ± 1.244E+06	MM

1044
1045
1046

Notes: The samples (n=11) above the horizontal black line are from Kaplan et al. (2017).

Table 3. ^{10}Be , ^{26}Al ages from Mt. Achnamar.

Sample name	^{10}Be Age $\pm 1\sigma$			^{10}Be Age $\pm 1\sigma$			^{10}Be Age $\pm 1\sigma$			^{26}Al Age $\pm 1\sigma$		
	St (yrs)	ext. err		Lm (yrs)	ext. err		LSDn (yrs)	ext. err		Lm (yrs)	ext. err	
MAR-11-22	13800 \pm 310	560		13400 \pm 300	540		12100 \pm 270	480		17500 \pm 1380	2160	
MAR-11-10	189400 \pm 2880	7300		183500 \pm 2790	6980		165500 \pm 2500	6130		180200 \pm 3610	18880	
MAR-11-18	5000 \pm 90	190		4800 \pm 90	180		4300 \pm 80	160		4900 \pm 370	590	
MAR-11-26	182300 \pm 2690	6980		176600 \pm 2600	6670		159400 \pm 2340	5870		179000 \pm 5120	19100	
MAR-11-30	51700 \pm 1220	2150		50100 \pm 1190	2070		45300 \pm 1070	1830		48400 \pm 1150	4800	
MAR-11-37	103700 \pm 1350	3840		100500 \pm 1300	3670		90900 \pm 1180	3240		96200 \pm 1950	9690	
MAR-11-14a	547900 \pm 6930	22390		529300 \pm 6660	21240		473400 \pm 5870	18300		439000 \pm 10220	52600	
MAR-11-14b	550700 \pm 6980	22530		532100 \pm 6710	21360		475800 \pm 5910	18410		454600 \pm 10690	54930	
MAR-11-17	6300 \pm 180	280		6100 \pm 180	270		5600 \pm 160	240		5100 \pm 520	710	
MAR-11-33	37500 \pm 490	1370		36400 \pm 480	1310		32900 \pm 430	1160		31200 \pm 1070	3160	
MAR-15-63	82 \pm 5	6		79 \pm 5	5		81 \pm 5	6				
MAR-15-89	15500 \pm 190	560		15100 \pm 180	540		13700 \pm 160	470				
MAR-15-57	12500 \pm 240	490		12100 \pm 240	470		10900 \pm 210	410				
MAR-15-58	11100 \pm 210	430		10700 \pm 210	410		9600 \pm 190	360				
MAR-15-59	6100 \pm 120	240		6000 \pm 110	230		5400 \pm 100	200				
MAR-15-62	4200 \pm 120	190		4100 \pm 120	180		3700 \pm 110	160				
MAR-15-107	3400 \pm 90	150		3300 \pm 90	140		2900 \pm 80	120				
MAR-15-108	3100 \pm 90	140		3000 \pm 90	130		2700 \pm 80	120				
MAR-15-101	9500 \pm 210	380		9200 \pm 200	370		8200 \pm 180	320				
MAR-15-102	14900 \pm 290	580		14500 \pm 280	560		13100 \pm 250	500				
MAR-15-105	12300 \pm 290	510		11900 \pm 280	490		10700 \pm 250	430				
MAR-15-110	610 \pm 32	38		600 \pm 31	37		520 \pm 27	32				
MAR-15-123	88800 \pm 1380	3360		86100 \pm 1340	3220		77900 \pm 1210	2850				
MAR-15-124	123800 \pm 2570	5020		120000 \pm 2490	4810		108400 \pm 2240	4260				
MAR-15-127	19600 \pm 380	770		19100 \pm 360	730		17200 \pm 330	650				
MAR-15-129	6100 \pm 150	250		5900 \pm 140	240		5400 \pm 130	220				
MAR-15-130	19600 \pm 370	760		19000 \pm 360	730		17200 \pm 320	650				
MAR-15-61	2900 \pm 680	690		2800 \pm 660	670		2400 \pm 580	590				
MAR-15-92	8900 \pm 500	590		8600 \pm 490	570		7700 \pm 440	500				
MAR-15-96	10100 \pm 620	710		9800 \pm 600	690		8800 \pm 540	610				
MAR-15-113	384600 \pm 7140	16010		372100 \pm 6890	15250		334200 \pm 6120	13300				
MAR-15-115	110100 \pm 2390	4510		106800 \pm 2320	4320		97000 \pm 2100	3850				
MAR-15-116	109000 \pm 3200	4960		105700 \pm 3100	4760		96000 \pm 2810	4250				
MAR-15-117	106200 \pm 2540	4480		103000 \pm 2470	4300		93600 \pm 2230	3830				
MAR-15-118	19100 \pm 650	920		18600 \pm 630	880		16900 \pm 570	790				
MAR-15-121	88500 \pm 1710	3500		85800 \pm 1660	3360		78000 \pm 1500	2990				
MAR-15-64	53 \pm 4	4		52 \pm 4	4		54 \pm 4	4				
MAR-15-65	79 \pm 9	9		76 \pm 8	9		78 \pm 9	9				
MAR-15-111	1070 \pm 25	44		1040 \pm 25	42		890 \pm 21	36				
MAR-15-142-T	2800 \pm 60	110		2700 \pm 60	110		2400 \pm 50	90				
MAR-15-143	880 \pm 22	37		850 \pm 21	35		730 \pm 18	30				
MAR-15-139	800 \pm 28	39		780 \pm 27	38		670 \pm 23	32				
MAR-15-142-H	720 \pm 29	37		700 \pm 28	36		600 \pm 24	31				
MAR-15-145	6400 \pm 120	250		6200 \pm 120	240		5600 \pm 110	210				
MAR-15-132	760 \pm 34	43		740 \pm 33	42		640 \pm 29	36				
MAR-15-133	1700 \pm 80	100		1700 \pm 80	90		1400 \pm 70	80				
MAR-15-137	18400 \pm 310	700		17800 \pm 300	670		16200 \pm 270	590				
MAR-15-94	9800 \pm 120	350		9500 \pm 120	340		8500 \pm 110	300				
MAR-15-97	9300 \pm 160	350		9000 \pm 150	340		8000 \pm 140	300				
MAR-15-87	330 \pm 10	15		320 \pm 10	15		290 \pm 9	13				
MAR-15-88	1100 \pm 20	40		1100 \pm 20	40		900 \pm 20	40				

1047
1048
1049
1050
1051

Notes: External errors (ext) provided in addition to internal (analytical) errors. The samples above the horizontal black line are from Kaplan et al. (2017), and ages are recalculated as discussed in Methods.

Table 4. ^3He ages from Mt. Achenar.

Sample name	^3He Age $\pm 1\sigma$		^3He Age $\pm 1\sigma$		^3He Age $\pm 1\sigma$	
	St (yrs)	ext. err	Lm (yrs)	ext. err	LSD (yrs)	ext. err
MAR-11-08	13200 \pm 1010	1770	13240 \pm 1010	1770	12090 \pm 920	1620
MAR-11-23	11800 \pm 720	1490	11820 \pm 720	1490	10770 \pm 660	1360
MAR-11-52	315900 \pm 7340	35510	315880 \pm 7330	35510	290120 \pm 6740	32620
MAR-11-48Green	108500 \pm 2950	12300	108550 \pm 2950	12300	99580 \pm 2710	11280
MAR-11-48Red	109100 \pm 3000	12370	109120 \pm 3000	12370	100100 \pm 2750	11350
MAR-11-21AL	23600 \pm 1260	2880	23600 \pm 1260	2880	21620 \pm 1150	2640
MAR-11-21CM	20800 \pm 1090	2530	20780 \pm 1090	2530	19030 \pm 1000	2320
MAR-11-35	98000 \pm 2600	11090	98030 \pm 2600	11090	90010 \pm 2390	10190
MAR-11-01	7000 \pm 630	990	7020 \pm 630	990	6460 \pm 570	910
MAR-11-02	7000 \pm 770	1090	7040 \pm 770	1090	6480 \pm 700	1000
MAR-11-09	11300 \pm 800	1480	11320 \pm 800	1480	10300 \pm 720	1340
MAR-15-112_avg	18000 \pm 520	2050	18000 \pm 520	2050	16470 \pm 470	1870
MAR_15_120	103700 \pm 1710	11530	103700 \pm 1710	11530	95780 \pm 1580	10650
MAR_11_41	157100 \pm 2670	17490	157110 \pm 2670	17490	145210 \pm 2470	16160
MAR_11_42	112600 \pm 1930	12540	112610 \pm 1930	12540	104060 \pm 1790	11590
MAR_15_126	179800 \pm 3030	20010	179810 \pm 3030	20010	164910 \pm 2780	18350
MAR_15_119	101000 \pm 1670	11240	101010 \pm 1670	11240	93310 \pm 1540	10380
MAR_15_125_2	135200 \pm 2230	15040	135210 \pm 2230	15040	123870 \pm 2050	13780
MAR_15_128_2	18600 \pm 370	2080	18630 \pm 370	2080	17040 \pm 340	1910
MAR_15_131_2	20500 \pm 400	2290	20490 \pm 400	2290	18750 \pm 360	2090
MAR_11_13	382000 \pm 6040	42450	381980 \pm 6040	42450	350400 \pm 5540	38940
MAR_11_15	223500 \pm 3660	24860	223530 \pm 3660	24860	205050 \pm 3360	22800
MAR_11_43	137600 \pm 2410	15330	137640 \pm 2410	15330	127150 \pm 2220	14160
MAR_15_122_2	115400 \pm 2380	12920	115400 \pm 2380	12920	106600 \pm 2200	11930
MAR-11-25	74800 \pm 3220	8830	74780 \pm 3220	8830	68590 \pm 2950	8100
MAR-11-25b	72700 \pm 4330	9090	72660 \pm 4330	9090	66640 \pm 3970	8340
MAR-11-27	197900 \pm 6350	22680	197930 \pm 6350	22680	181680 \pm 5830	20820
MAR-11-28	212700 \pm 6680	24340	212730 \pm 6680	24340	195270 \pm 6130	22340
MAR-11-29	60000 \pm 2840	7190	60020 \pm 2840	7190	55040 \pm 2610	6590
MAR-11-31	38100 \pm 2120	4700	38100 \pm 2120	4700	34900 \pm 1940	4300
MAR-11-32	14300 \pm 1530	2190	14270 \pm 1530	2190	13020 \pm 1400	2000
MAR-11-34	51400 \pm 2530	6190	51420 \pm 2530	6190	47140 \pm 2320	5680
MAR-11-36	57800 \pm 2960	7010	57800 \pm 2960	7010	53010 \pm 2720	6430
MAR-11-38	108700 \pm 4220	12680	108660 \pm 4220	12680	99780 \pm 3880	11640
MAR-11-39	118100 \pm 4360	13700	118080 \pm 4360	13700	108430 \pm 4000	12580
MAR-11-40	39900 \pm 1670	4690	39870 \pm 1670	4690	36560 \pm 1530	4310

1052
1053

1054

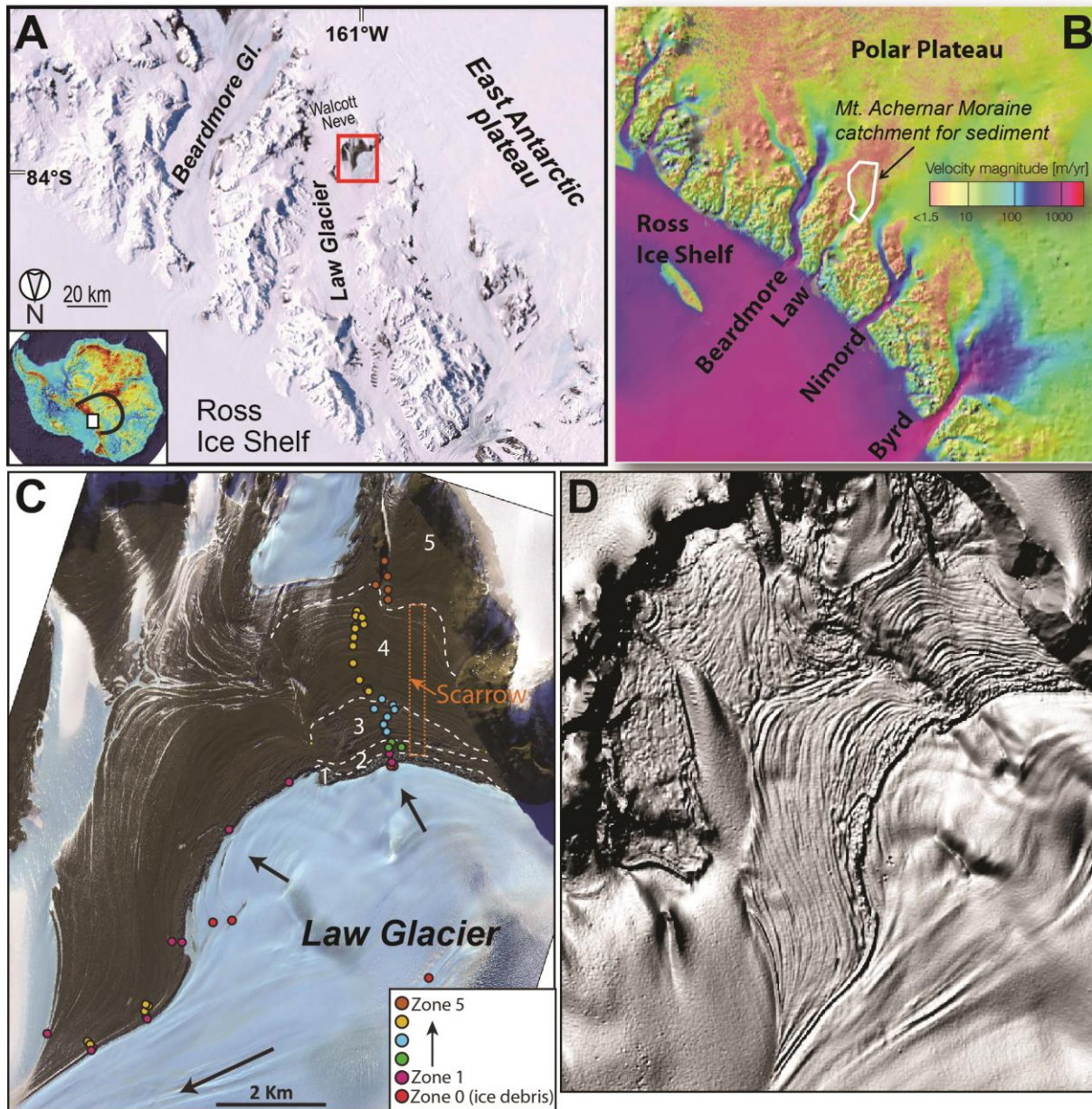
1055

1056

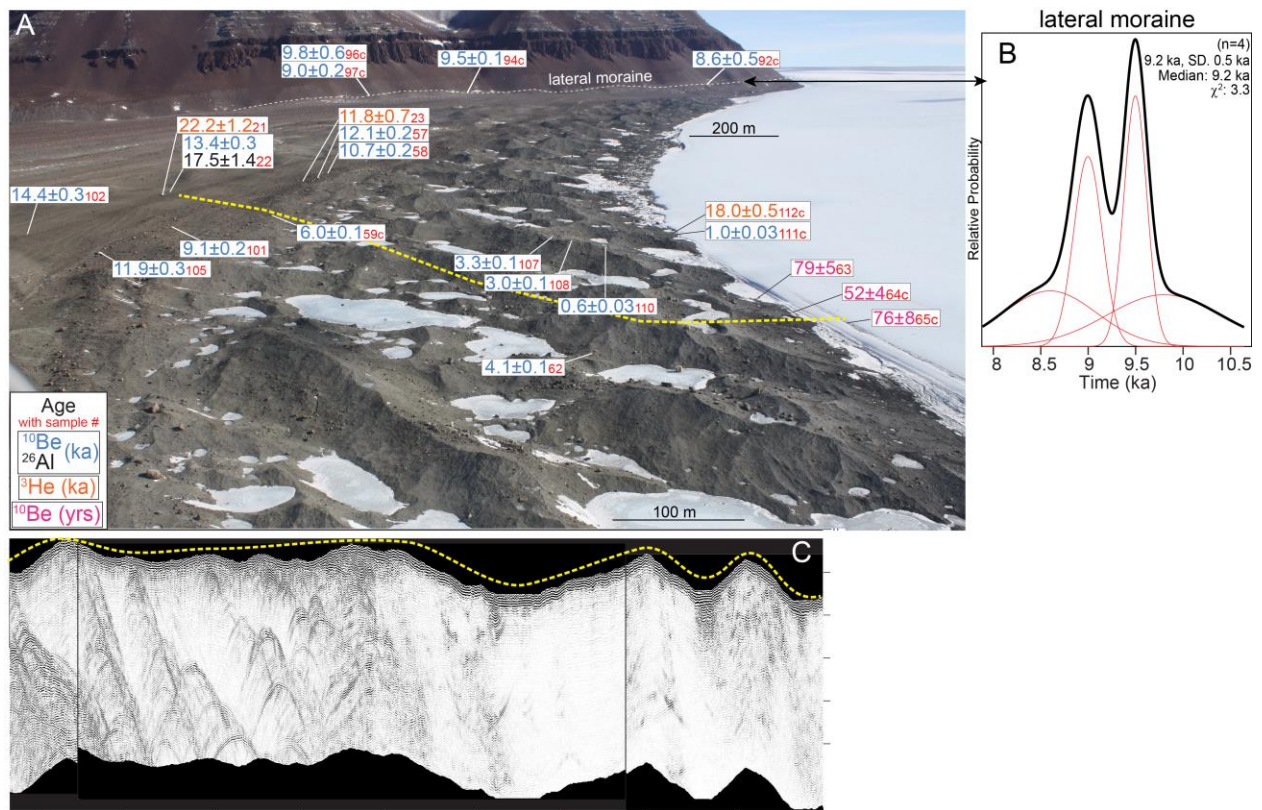
1057

1058

Notes: External errors (ext) provided in addition to internal (analytical) errors. The samples above the horizontal black line are from Kaplan et al. (2017), and ages are recalculated as discussed in Methods. For samples measured twice, on figures we show an average age and the higher of the two respective errors.



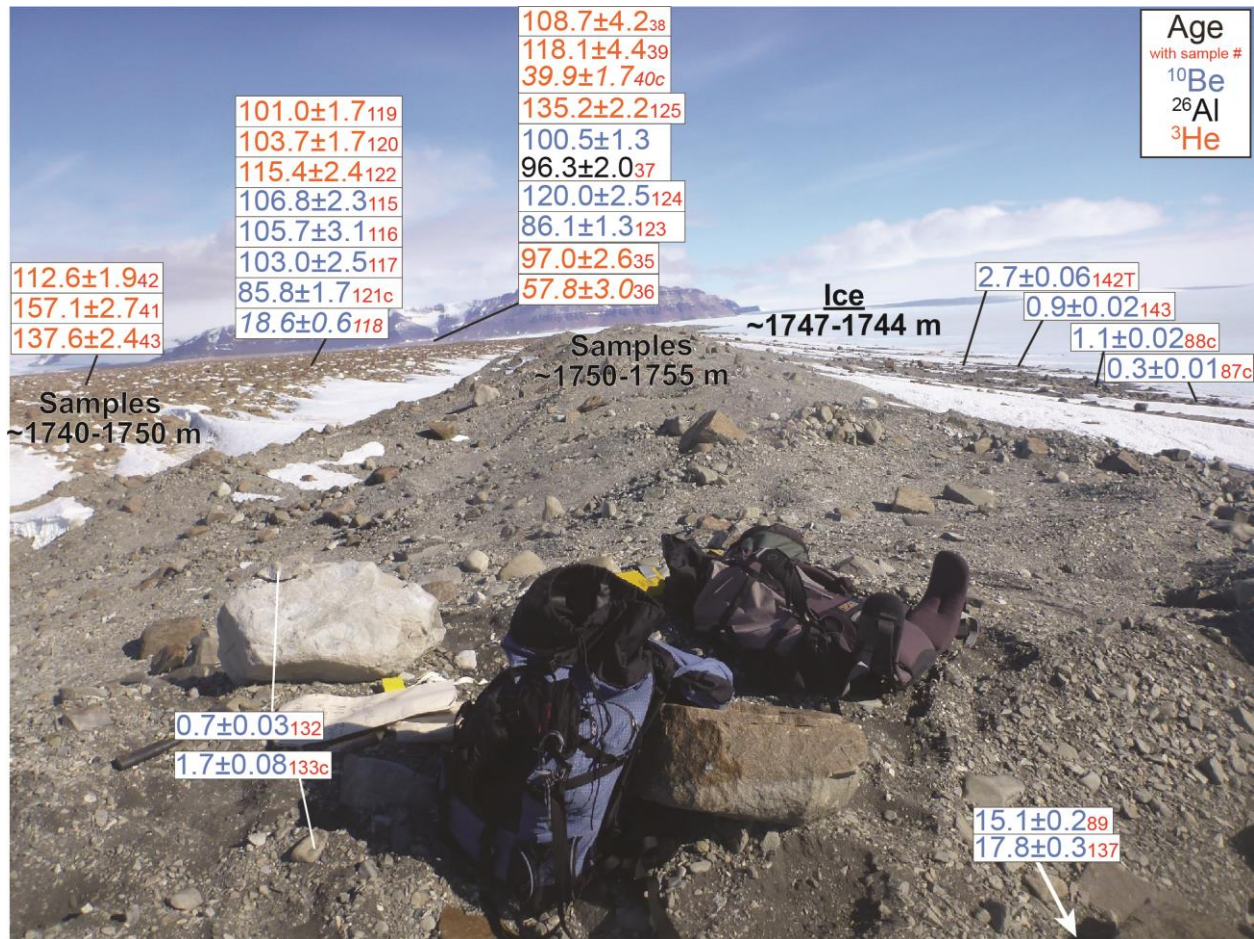
1059
 1060 Figure 1. Setting of the Mt. Acheron area. A) Mt. Acheron moraine sits at the head of Law Glacier
 1061 (within red box) where unconstrained flow off of the East Antarctic plateau becomes constrained
 1062 through Transantarctic Mountains. B) Ice surface velocities and sediment catchment area for the
 1063 Mt. Acheron area (Bader et al. 2017; Graly et al., 2018b). C) The entire moraine complex along
 1064 with locations of sediment (till) samples for study of provenance changes (Bader et al., 2017) and
 1065 soil geochemistry (Graly et al., 2017). Also shown are zones (in white) defined in Bader et al.
 1066 (2017), the general area of study by Scarrow et al. (2014), and ice flow directions with arrows.
 1067 Note the ice flow is steered away from the main trunk glacier, where it is then trapped in the
 1068 embayment (Kassab et al. 2020). D) Image of the Acheron moraine and surrounding area, from
 1069 Antarctic REMA (Reference Elevation Model of Antarctica) Explorer (Howat et al., 2019).



1082
 1083 Figure 3. Focus on the best-dated Zones 1 and 2, looking west with the Law Glacier on the right.
 1084 Headwall of Mt. Achnar shown in background. Four ^{10}Be ages on samples along the lateral
 1085 moraine, date to 9.2 ± 0.5 ka and record a high surface for ice flowing off the plateau, which is
 1086 seen in the upper right. GPR radargram profile below the photo is from Kassab et al. (2020), and
 1087 more or less follows the yellow-dashed line. Dipping stacked and scattered hyperbolas are
 1088 inferred to represent planes of debris and cobbles/boulders causing point reflectors, respectively.
 1089 Figure 6 provides additional photos of the lateral moraine with samples.
 1090

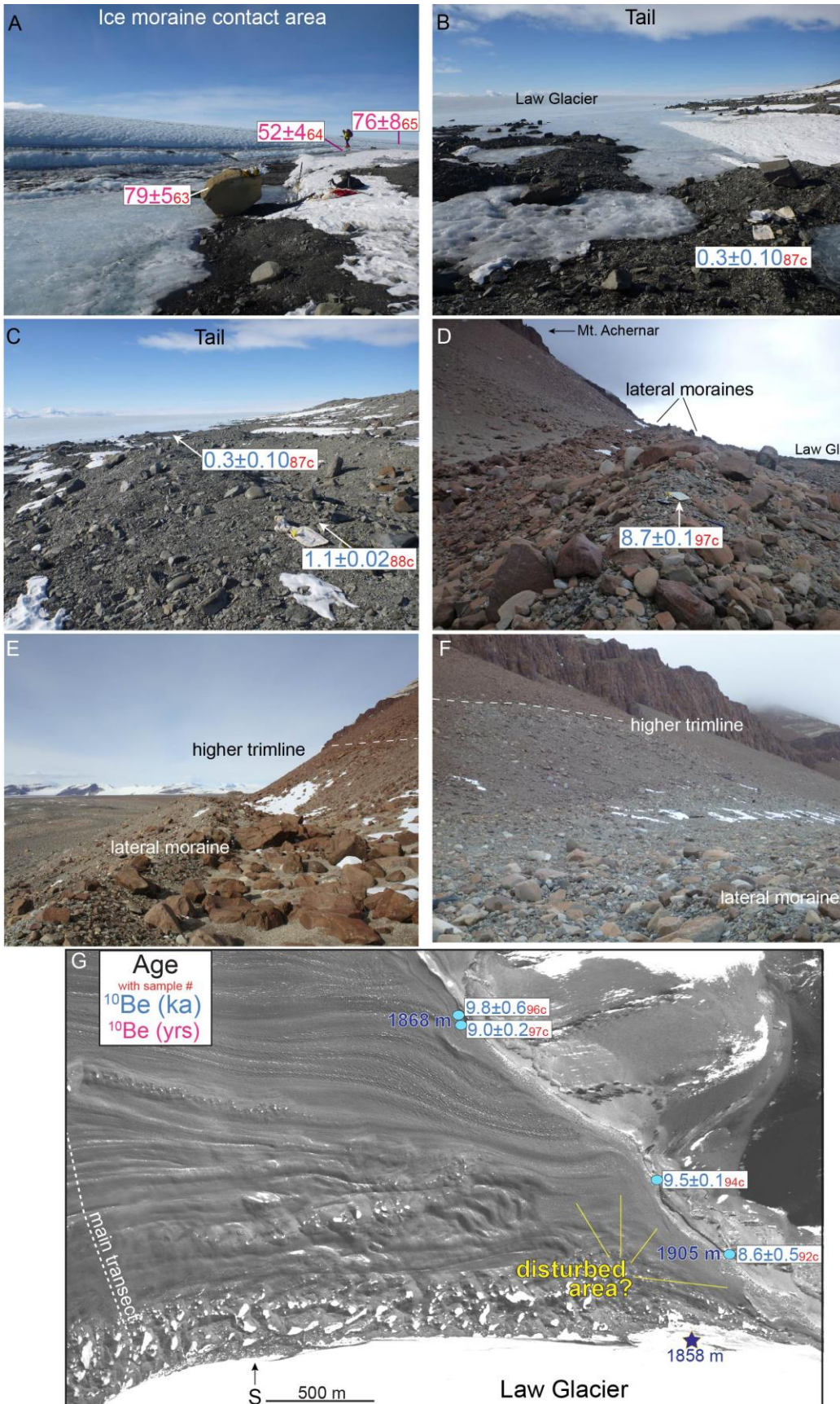


1091
 1092 Figure 4. Similar to Figure 3, with photos focusing on Zones 2 to 4 and cosmogenic exposure ages.
 1093 Top panel focuses on Zone 2, with the Law Glacier (Fig. 3) on right side. Middle panel focuses on
 1094 Zones 2 and 3 including moraines dated to MIS 2 time; the average and standard deviation are
 1095 19.3±0.8 ka excluding the one outlier of 5.9±0.1. Bottom panel focuses on inner Zone 4 and
 1096 samples dating to <100 ka. Mt Achnar headwall is in the background. In each subsequent panel,
 1097 some overlap in exposure ages is shown on right side.
 1098

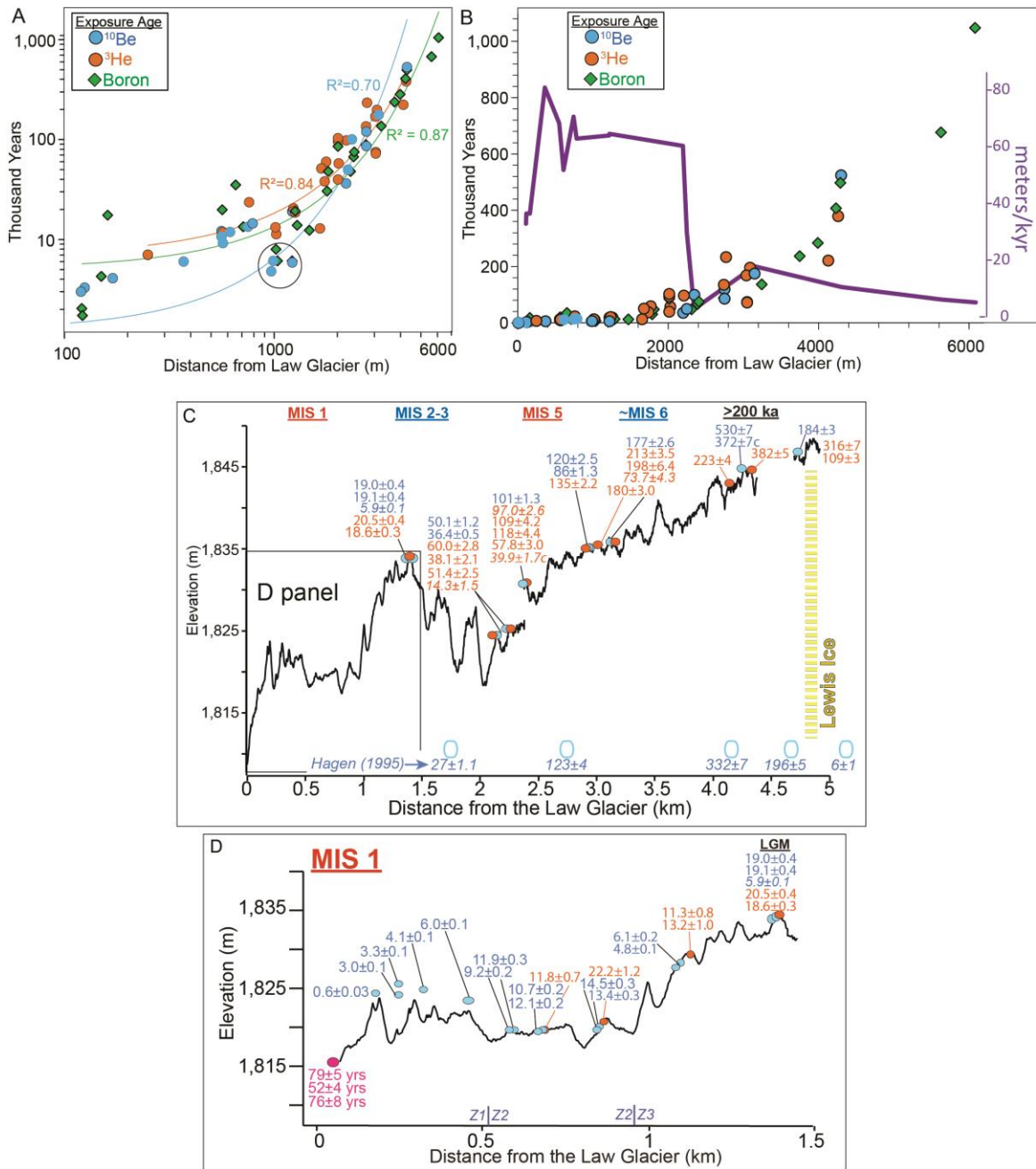


1099
 1100
 1101
 1102
 1103
 1104
 1105
 1106
 1107
 1108

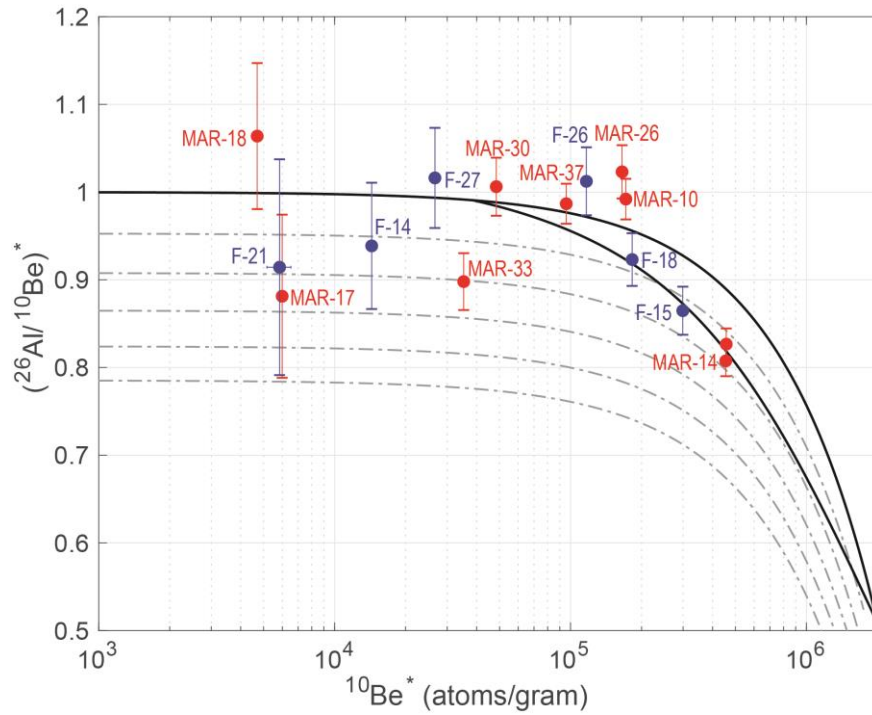
Figure 5. A focus on the tail area, with view looking southwest, towards Mt. Achernar. Law Glacier is on the right. Note relatively oxidized sediments on the left side of the photo, which date to MIS 6 and 5 except for 1 outlier of ~18.6 ka. Also shown are MIS 5 ages (~135.2 to ~86.1 ka) from the main area of focus (Fig. 2B), which is in the background. All are boulder ages except if labelled "c" (cobble size). Two outliers are italicized. See Figure 6 for photos that focus on the right side of image; both the ~0.3 and ~0.9 ka ages are slightly closer to the present margin, compared with the ~1.1 and ~2.7 ka ages.



1110 Figure 6. Photos that provide context of geomorphology and age data. A) Three ^{10}Be ages near
1111 the moraine/ Law Glacier boundary. Person for scale. In this panel the three ages are in years, in
1112 all other panels they are in ka. B) and C) A focus on the tail area and samples MAR-15-87 (ice
1113 margin) and -88 (+4 m). D) The lateral moraine, with two apparent ridges. E) The lateral
1114 moraine and trimline, close to (NW of) sample MAR-15-92c (panel G). The tallest boulders are
1115 ~1 m in height and we estimate the trimline is about 15-20 m higher. F) The lateral moraine and
1116 trimline, by MAR-15-98c (panel G). We estimate the trimline is <10 m higher. G) The area near
1117 the lateral moraine with ^{10}Be ages (all cobbles). We also show the elevation difference between
1118 the Law Glacier (1858 m), lateral moraine (~1905 m), and towards the south (1868 m). Note the
1119 area next to the lateral moraine is smoother without distinct ridges, as exists to the left (east)
1120 closer to the area of the main transect (white-dashed line, Fig. 2). We infer disturbances within
1121 ~500 m of the lateral moraine due to the rise in surface by ~10-9 ka and when the trimline
1122 formed.

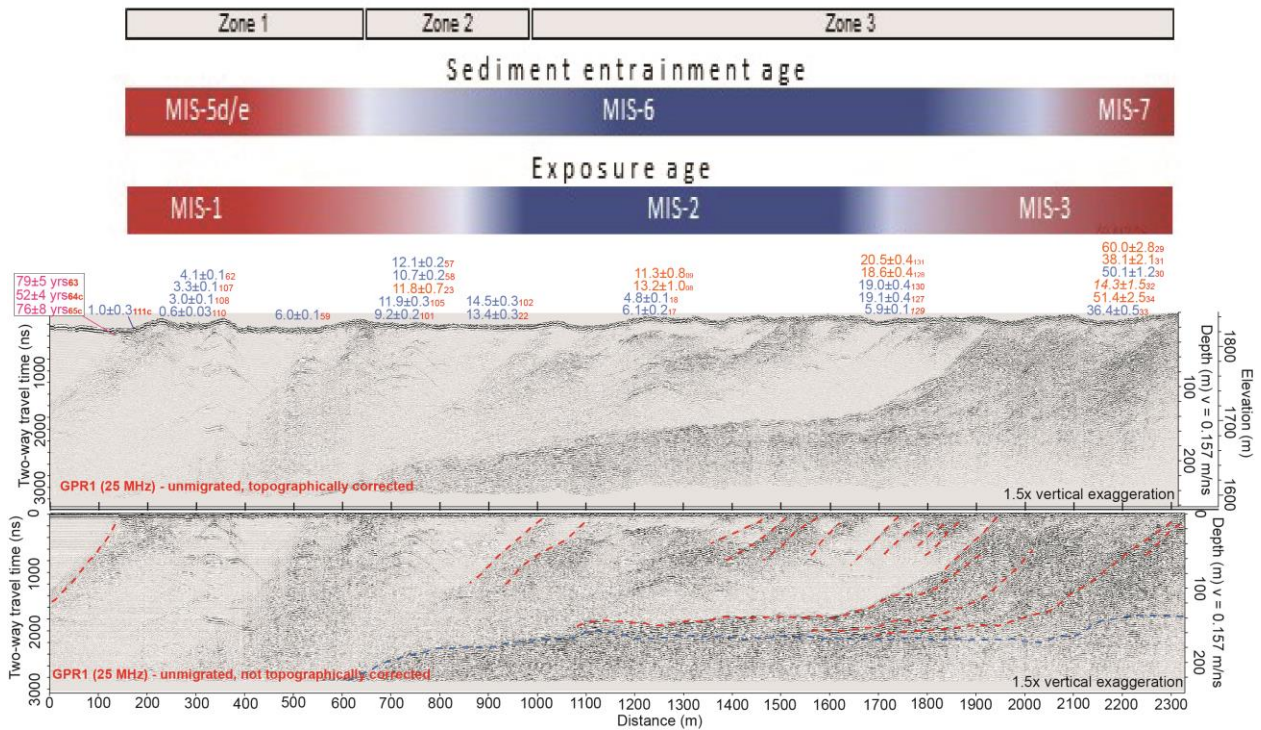


1123
 1124 Figure 7. ^{10}Be - ^3He -Boron exposure ages with distance from the Law Glacier along the main
 1125 transect (white-dashed line, Fig. 2). **Panels A, B**) Left side is plotted as log-log plot. Three
 1126 respective exponential relations demonstrate there is a steady increase in age from the active
 1127 margin. Within ~2200 m (~50 ka) from the Law Glacier, if the relation is represented by a linear
 1128 line, the r^2 is ~0.8 (^{10}Be) or ~0.6 (^3He). Boron ages are from Graly et al. (2018a). Circle marks
 1129 younger sediment dated, where ^{10}Be - ^{26}Al -Boron exposure ages all indicate exposure for less time.
 1130 In panel B, approximate average accretion rate based on ^{10}Be and the two oldest Boron ages at
 1131 ~5600-6100 m. **Panels C, D**) Topographic profiles from Bader et al. (2017) and Kaplan et al.
 1132 (2017). In panel C, the ages from Hagen (1995) are at the bottom because it is not clear how they
 1133 align with the main transect. MIS labels are approximately located with distance. For simplicity,
 1134 ^{26}Al ages are not shown. In Panel D, Zones 1 to 3 (Z1-Z3) are shown along bottom.



1135
 1136
 1137
 1138
 1139
 1140
 1141
 1142
 1143

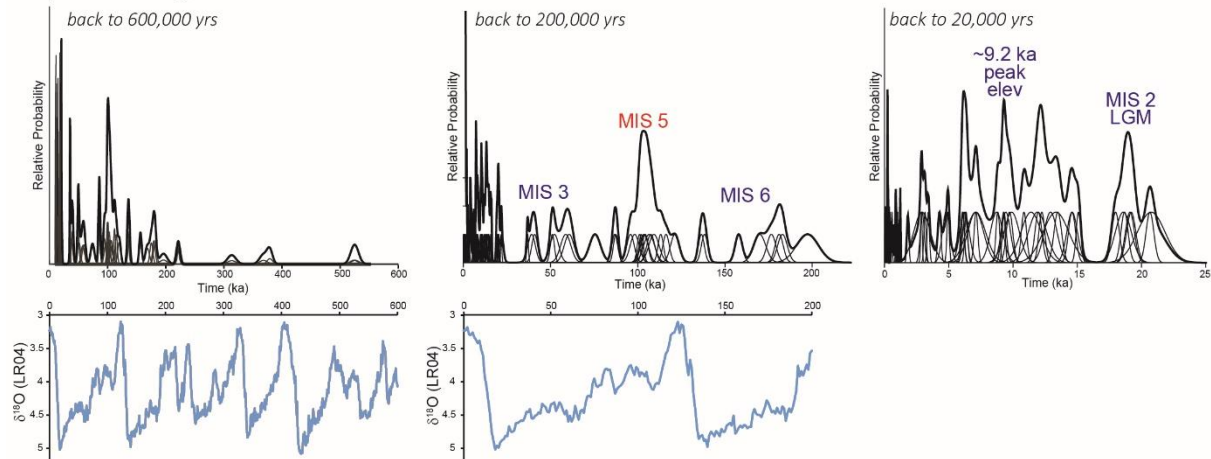
Figure 8. Plot of $^{26}\text{Al}/^{10}\text{Be}$ ratios versus ^{10}Be concentrations, with data colored in blue and red from Hagen (1995) and Kaplan et al. (2017), respectively, recalculated with updated systematics. MAR-11-22 is not shown on the plot due to its high $^{26}\text{Al}/^{10}\text{Be}$ value (Table 1). The first and last parts of each sample name are shown next to analyses. The ratios are standardized (*) to 6.75, the Be-10 concentrations are relative to 07KNSTD and sea level high latitude (Balco et al., 2008). Error bars are 1σ analytical uncertainty.



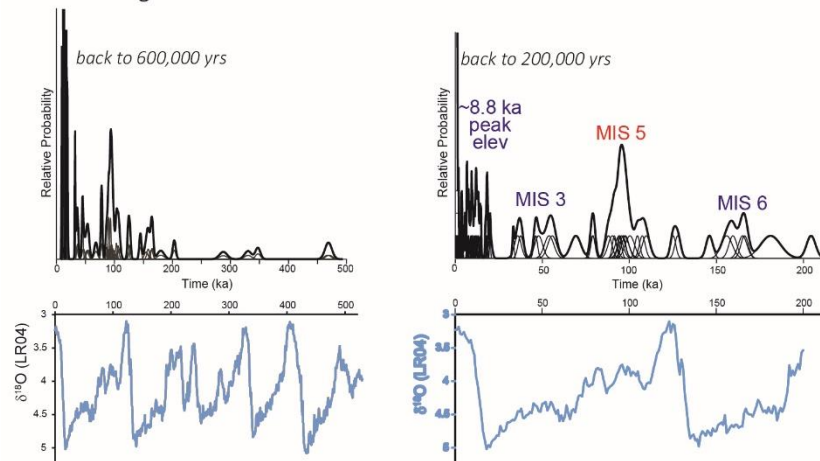
1144
1145
1146
1147
1148
1149
1150
1151
1152
1153
1154

Figure 9. Ground Penetrating radar (GPR, 25MHz) with approximate locations of ^{10}Be - ^3He above the topographically corrected surface. Ages are shifted slightly so as to be at their approximate location along GPR transect. The upper panel is the processed radargram and the lower panel has interpretations including red-dashed lines as debris planes. Kassab et al. (2020) interpreted the blue-dashed line, which represents a continuous subhorizontal reflector, to be the bedrock surface at ~140 m to >220 m below. Above the GPR data, we show both maximum sediment entrainment age (Graly et al., 2020, Kassab et al. 2020) and surface exposure ages. Boundaries between MIS are fuzzy given ranges of ages. Kassab et al. (2020) also presented GPR analyses for inner Zone 4, with exposure ages $\geq 100\text{ka}$, but they found a lack of consistent GPR reflections. For simplicity, ^{26}Al ages are not shown.

St/Lm scaling



LSD scaling



1155
1156
1157
1158
1159
1160
1161
1162
1163

Figure 10. ^{10}Be - ^{26}Al - ^3He ages compared with benthic $\delta^{18}\text{O}$ stack (Lisiecki and Raymo, 2004). Top panels include ages with St/Lm scaling (difference not discernable at the scale shown). During MIS 5, a concentration of ages occurs at 120-100 ka excluding "outlier" ages <90 ka from the same sites (Fig. 5). Taken at face value these ages overlap with MIS5c or 5c-d. Bottom panels include exposure ages calculated with the LSDn scaling (Table 1,3) method, which are ~10-12% lower than those calculated using St/Lm.



Click here to access/download
e-Component/Supplementary data
Tables 1 to 4 Kaplan et al.xlsx

